1 **A conserved function for pericentromeric satellite DNA**

2 Madhav Jagannathan[1], Ryan Cummings[1, 3], Yukiko M. Yamashita[1, 2, 3, *]

3 [1]Life Sciences Institute, University of Michigan.

4 [2]Department of Cell and Developmental Biology, University of Michigan.

5 [3]Howard Hughes Medical Institute, University of Michigan.

6 *Correspondence to: yukikomy@umich.edu

Abstract:

A universal and unquestioned characteristic of eukaryotic cells is that the genome is divided into multiple chromosomes and encapsulated in a single nucleus. However, the underlying mechanism to ensure such a configuration is unknown. Here we provide evidence that pericentromeric satellite DNA, which is often regarded as junk, is a critical constituent of the chromosome, allowing the packaging of all chromosomes into a single nucleus. We show that the multi AT-hook satellite DNA binding proteins, *D. melanogaster* D1 and mouse HMGA1, play an evolutionarily conserved role in bundling pericentromeric satellite DNA from heterologous chromosomes into 'chromocenters', a cytological association of pericentromeric heterochromatin. Defective chromocenter formation leads to micronuclei formation due to budding from the interphase nucleus, DNA damage and cell death. We propose that chromocenter and satellite DNA serves a fundamental role in encapsulating the full complement of the genome within a single nucleus, the universal characteristic of eukaryotic cells.

Introduction

Satellite DNA is AT-rich, non-coding, repetitive DNA that is abundant in centromeric and pericentromeric heterochromatin. Unlike the satellite DNAs that comprise the vast majority of natural centromeres (Willard, 1990; Sun et al., 1997; 2003), the role of pericentromeric satellite DNA remains obscure: although function for a few satellite DNA repeats has been implied in certain cellular processes such as meiotic segregation of achiasmatic chromosomes, X chromosome dosage compensation and formation of lampbrush-like loops on the Y chromosome during male meiosis (Yunis and Yasmineh, 1971; Bonaccorsi et al., 1990; Dernburg et al., 1996; Menon et al., 2014), a unifying theme for pericentromeric satellite DNA function remains elusive. Moreover, highly divergent satellite DNA sequences even among closely-related species has led to the idea that satellite DNA does not serve a conserved function and is mostly a selfish element or junk (Doolittle and Sapienza, 1980; Walker, 1971). Pericentromeric satellite DNA repeats are proposed to be sources of genomic instability, as their misexpression is associated with the formation of genotoxic R-loops and DNA damage (Zhu et al., 2011; Zeller et al., 2016; Zeller and Gasser, 2017). Most studies on pericentromeric heterochromatin have focused on the mechanisms to repress satellite DNA transcription, and accordingly, a clear rationale for the existence of most pericentromeric satellite DNA is still lacking.

Cytologically, it is well documented that pericentromeric satellite DNA from multiple chromosomes is clustered into chromocenters in interphase nuclei in diverse eukaryotes including *Drosophila*, mouse and plants (Figure 1A) (Jones, 1970; Pardue and Gall, 1970; Gall et al., 1971; Fransz et al., 2002). While multiple factors such as epigenetic modifications and transcription of repetitive DNA from pericentromeric DNA sequences are known to be required for chromocenter formation (Peters et al., 2001; Probst et al., 2010; Bulut-Karslioglu et al., 2012; Pinheiro et al., 2012; Hahn et al., 2013), the ultimate consequences of disrupted chromocenter formation has never been addressed, leaving the function of chromocenters unknown.

In this study, we explored the role of pericentromeric satellite DNA/chromocenters by studying multi-AT-hook proteins, D1 from *Drosophila melanogaster* and HMGA1 from mouse. D1 and HMGA1 are known to bind specific pericentromeric satellite DNA, and we show that

these proteins are required for chromocenter formation. When chromocenters are disrupted in the absence of these proteins, cells exhibited a high frequency of micronuclei formation, leading to DNA breakage and cell death. We show that micronuclei are formed during interphase, by budding from the nucleus. We further show that D1 binding to the target DNA sequence is sufficient to bring it to the chromocenter. High-resolution imaging revealed chromatin threads positive for D1/HMGA proteins and satellite DNA that connect heterologous chromosomes. Taken together, we propose that chromocenter formation via bundling of satellite DNA from heterologous chromosomes functions as a mechanism to encapsulate the full complement of the genome into a single nucleus. We suggest that satellite DNA function as a critical constituent of chromosomes and may serve an evolutionarily conserved role across eukaryotic species.

Results

The multi-AT-hook satellite DNA binding proteins, *Drosophila* D1 and mouse HMGA1, localize to chromocenters.

D1 in *Drosophila melanogaster* and HMGA1 in mouse are multi-AT-hook proteins; D1 contains 10 AT-hooks, HMGA1 contains 3 AT-hooks and both proteins contain C-terminal acidic domains (Aulner et al., 2002). D1 and HMGA1 are known to bind the *Drosophila* $\{AATAT\}_n$ satellite DNA (~8% of the *Drosophila* male diploid genome) and mouse major satellite DNA (~6% of the mouse genome), respectively (Goodwin et al., 1973; Rodriguez Alfageme et al., 1980; Levinger and Varshavsky, 1982b; a; Lund et al., 1983). The $\{AATAT\}_n$ satellite is distributed across 11 loci on multiple chromosomes as visualized by DNA fluorescence in situ hybridization (FISH) on mitotic chromosome spreads (Figure 1B) (Lohe et al., 1993; Jagannathan et al., 2017). However, it is typically clustered into a few foci in *Drosophila* interphase nuclei, colocalizing with the D1 protein (Figure 1C). The D1/$\{AATAT\}_n$ foci stained positively for H3K9me2 in interphase nuclei (Figure 1C), a well-established characteristic of constitutive heterochromatin/chromocenters (Guenatri et al., 2004). Consistently, D1 localized near the centromere (marked by *Drosophila* CENP-A, Cid) on mitotic chromosome spreads (marked by phosphorH3 S10) (Figure 1D). These results suggest that D1 is a chromocenter-localizing protein, via its binding to the $\{AATAT\}_n$ satellite DNA.

81 The mouse HMGA1 protein was originally identified as an abundant non-histone
82 component of mammalian chromatin (Goodwin et al., 1973; Lund et al., 1983) with subsequent
83 studies demonstrating its binding to satellite DNA (Strauss and Varshavsky, 1984; Radic et al.,
84 1992). Mouse major satellite, which is present in pericentromeric regions of all chromosomes
85 (Figure 1E) (Lyon and Searle, 1989), clustered into DAPI-dense chromocenters positive for
86 HMGA1 protein (Figure 1F, Figure 1-figure supplement 1A, B), revealing an analogous
87 relationship to D1/{AATAT}$_n$ satellite in *Drosophila*. Interestingly, we found that *Drosophila*
88 D1 protein localizes to major satellite/chromocenters when ectopically expressed in multiple
89 mouse cell lines (Figure 1G, Figure 1-figure supplement 1C, D), suggesting that D1 and
90 HMGA1 may possess an orthologous and conserved function as satellite DNA/chromocenter-
91 binding proteins.

92

93 **D1 and HMGA1 are required for organizing chromocenters**

94 We next examined the effects of *D1* mutation and siRNA-mediated knockdown of
95 HMGA1 on chromocenters. We used two *D1* alleles, $D1^{LL03310}$ and $D1^{EY05004}$, which we show to
96 be protein null alleles, evidenced by near-complete loss of anti-D1 antibody staining (Figure 1-
97 figure supplement 2A-C). When these alleles were combined with the D1 deficiency allele,
98 Df(3R)BSC666, it led to severe declustering of {AATAT}$_n$ satellite DNA (Figure 1H-J, Figure
99 1-figure supplement 2D-E), suggesting that D1 is required for clustering of pericentromeric
100 satellite DNA into chromocenters. We observed D1's requirement for chromocenter formation in
101 multiple cell types (Figure 1-figure supplement 2F-I), but we largely focused on spermatogonial
102 cells, where the phenotypes (such as cell death) were most penetrant and severe.

103

104 We also examined the requirement for HMGA1 in mouse chromocenter formation.
105 Following siRNA-mediated knockdown of HMGA1, which led to near complete loss of HMGA1
106 protein (see Figure 2D, E and Figure 2-figure supplement 1A-B, D-E for efficiencies of HMGA1
107 knockdown), we observed chromocenter disruption in multiple mouse cell lines (Figure 1K-M,
108 Figure 1-figure supplement 2J-L). These results suggest that D1 and HMGA1 have an
109 orthologous function to organize pericentromeric satellite DNA into chromocenters.

110

111 **Loss of D1/HMGA1 leads to micronuclei formation.**

112 To explore the function of chromocenters and satellite DNA, we examined the effects of
113 *D1* mutation/HMGA1 knockdown, which showed strikingly similar phenotypes. We found that
114 *D1* mutation as well as siRNA-mediated HMGA1 knockdown in multiple mouse cell lines
115 resulted in a significant increase in micronuclei formation (Figure 2A-F, Figure 2-figure
116 supplement1A-F).

117

118 Micronuclei are known to have compromised nuclear envelope integrity, leading to DNA
119 damage and catastrophic chromosomal rearrangement therein (Crasta et al., 2012; Hatch et al.,
120 2013). Therefore, we first examined a possible defect in nuclear envelope integrity in *D1* mutant.
121 We found that loss of D1 led to breaching of the nuclear envelope both in major and micronuclei,
122 visualized by the cytoplasmic leakage of nuclear GFP (nlsGFP) (Figure 2G-I), suggesting that
123 nuclear envelope integrity might be generally compromised. Consistently, we observed
124 mislocalization of nuclear envelope proteins in *D1* mutant spermatogonia. We frequently
125 observed that lamin surrounded the nucleus incompletely in *D1* mutant (1.9% in control (n=52)
126 and 68.9% in *D1* mutant (n=58)) (Figure 2J, K, arrows indicate lamin-negative regions on the
127 nuclear membrane). We also observed cytoplasmic 'holes', which resemble the nucleus in that
128 they exclude cytoplasmic proteins such as Vasa (Figure 2K, arrowhead), but are devoid of
129 nuclear lamin (Figure 2K, arrowhead). These 'holes' were often surrounded by an ER marker,
130 which normally surrounds the nuclear envelope (Figure 2J) (Dorn et al., 2011). Similarly, Otefin,
131 an inner nuclear membrane LEM-domain protein (Barton et al., 2014), also showed perturbed
132 localization (2.7% in control (n=109) and 24.5% in *D1* mutant (n=106)) (Figure 2L, M, arrows
133 indicate lamin/Otefin negative regions on the nuclear envelope while the arrowhead indicates
134 Otefin-positive micronuclei). Taken together, these results show that *D1* mutant cells exhibit
135 compromised nuclear envelope integrity, which is associated with micronuclei formation.

136

137 **Loss of D1/HMGA1 leads to accumulation of DNA damage**

138 It has been shown that defects in nuclear envelope integrity can lead to extensive DNA
139 damage in the major nucleus and micronuclei (Crasta et al., 2012; Hatch et al., 2013; Zhang et
140 al., 2015; Denais et al., 2016; Raab et al., 2016). Nuclear envelope defects and extensive DNA
141 damages therein lead to catastrophic chromosomal breaks/rearrangements termed chromothripsis
142 (Crasta et al., 2012; Hatch et al., 2013). Such catastrophic DNA breaks/rearrangements are
143 speculated to lead to tumorigenesis (Hatch and Hetzer, 2015).

144

145 Consistent with defective nuclear envelope integrity, we observed extensive DNA
146 damage (revealed by γ-H2Av) in both major and micronuclei (Figure 3A-F, arrows point to
147 damaged DNA in micronuclei in B and D). Likely as a result of DNA damage and defective
148 nuclear envelope integrity, *D1* mutant testes rapidly degenerated (Figure 3 –figure supplement
149 1A, B). When *Omi*, a gene required to promote germ cell death (Yacobi-Sharon et al., 2013), was
150 knocked down in *D1* mutant testes, it restored the cellularity in *D1* mutant testis (Figure 3-figure
151 supplement 1C-D), but the surviving cells showed a dramatic increase in DNA damage (Figure
152 3-figure supplement 1E-F). Under these conditions, we observed that surviving germ cells in *D1*
153 mutant testes showed a high frequency of chromosome breaks compared to control, revealed by
154 FISH on metaphase chromosome spreads from spermatocytes (3.7% in control (n=27) vs. 15.8%
155 in *D1* mutant (n=57)) (Figure 3G, H, arrowheads indicate sites of chromosome breaks). These
156 results show that loss of D1/HMGA1 results in compromised nuclear envelope integrity, leading
157 to extensive DNA damage and chromosomal breaks.

158

159 **Micronuclei formation in *D1* mutant/HMGA1 knockdown cells is due to budding from the**
160 **nucleus during interphase.**

161 It has been shown that micronuclei form by lagging chromosomes (Crasta et al., 2012).
162 Thus, we examined whether *D1* mutation/HMGA1 knockdown resulted in mitotic chromosome
163 segregation errors, causing micronuclei formation. However, we did not observe an increase in
164 lagging chromosomes in *D1* mutant spermatogonia or HMGA1-depleted mouse cells (Figure 4 –
165 figure supplement 1A-G), suggesting an alternative route for micronuclei formation. Instead,
166 time-lapse live observation showed that micronuclei formed by budding from the interphase
167 nucleus both in *Drosophila* spermatogonia and mouse cells (Figure 4A-D). In *Drosophila*

168 spematogonia, nuclear contents were visualized by a GFP-tagged nuclear protein, Df31, and
169 RFP-tagged histone H2Av. Control cells stably maintained nuclear contents for a prolonged time
170 period (only 1 event of nuclear blebbing without concurrent micronuclei formation (as detected
171 by H2Av) over 1552 minutes of live imaging) (Figure 4A). In contrast, *D1* mutant cells showed
172 budding off of nuclear contents and micronuclei formation in interphase (15 nuclear breaches
173 with 8 micronuclei formed over 3427 minutes of live imaging with a total budding duration of
174 172 minutes) (Figure 4B). Similarly, live imaging in mouse cells using the Hoechst DNA dye
175 revealed that HMGA1 knockdown also resulted in micronuclei formation during interphase
176 (siControl – no micronuclei formation over 253 minutes of live observation, siHMGA1 – 3
177 micronuclei formed by budding over 5962 minutes of live imaging with a total budding duration
178 of 310 minutes) (Figure 4C, D). These results show that micronuclei in *D1* mutant/HMGA1-
179 knockdown cells are generated during interphase, via budding from the nucleus.

180

181 **D1 bundles satellite DNA from multiple chromosomes to form chromocenter**

182 Based on the above results, we postulated that chromocenter formation, i.e. clustering of
183 satellite DNA from multiple chromosomes, might be a mechanism to bundle heterologous
184 chromosomes together to prevent individual chromosomes from floating out of the nucleus. In
185 this manner, the full set of chromosomes may be retained within a single nucleus. In the absence
186 of chromocenter formation, individual chromosomes may bud off the nucleus, leading to
187 micronuclei formation.

188

189 Previous *in vitro* experiments indicated that HMGA1 is capable of crosslinking multiple
190 DNA strands with individual AT-hooks binding AT-rich DNA strands (Vogel et al., 2011).
191 Bundling of DNA in this manner by D1/HMGA1 could explain how pericentromeric satellite
192 DNA from multiple chromosomes may be clustered to form chromocenters. A few lines of
193 evidence support this idea. When *Drosophila* D1 was expressed in mouse cells, it localized to the
194 chromocenter as described above (Figure 1G), and its overexpression enhanced chromocenter
195 formation in a dose-dependent manner (Figure 5A-C): the higher the amount of D1 that was
196 expressed in mouse cells, the fewer chromocenters per cell was observed (i.e. more clustering).
197 These results suggest that D1 is sufficient to bundle its binding target, tethering it to

198 chromocenter. Consistent with this idea, we found that artificial tethering of D1 protein to
199 euchromatic LacO repeat DNA sequences was sufficient to bring LacO repeats to the
200 chromocenter. D1 protein or D1-LacI fusion protein was expressed in a *Drosophila* strain in
201 which LacO repeats are inserted in the distal regions of the 2nd chromosome (Figure 5D, arrows).
202 In control spermatogonial cells expressing wild type D1, LacO repeats were observed far away
203 from the $\{AATAT\}_n$ satellite foci/chromocenters (Figure 5E, G, arrow indicates site of LacO
204 repeats in interphase nucleus). However, in cells expressing the LacI-D1 chimeric protein, we
205 observed recruitment of the LacO repeats close to $\{AATAT\}_n$/chromocenters (Figure 5F, G,
206 arrow indicates site of LacO repeats recruited to the chromocenter), demonstrating that D1's
207 binding to a DNA sequence is sufficient to incorporate the target sequence into chromocenters.

208

209 Although it cannot be visualized how DNA strands from multiple chromosome might be
210 bundled in these interphase chromocenters, deconvolution microscopy of D1/HMGA1 proteins
211 on early mitotic chromosomes revealed proteinaceous threads between chromatin in the process
212 of condensation (Figure 6A, B, arrows indicate D1/HMGA1 threads), which we speculate
213 contributed to bundling of chromosomes in the previous interphase. These threads were also
214 detectable by DNA FISH against $\{AATAT\}_n$ and the mouse major satellite (Figure 6C, D, dotted
215 lines are alongside the satellite DNA threads), suggesting that satellite DNA bound by
216 D1/HMGA1 can form threads. These threads likely connect heterologous chromosomes, as we
217 see threads between chromosomes that are clearly distinct in their morphology (e.g. Figure 6C).
218 These D1/HMGA1 threads are reminiscent of 'DNA fibers', which were observed among mitotic
219 chromosomes, although their function has never been appreciated (Takayama, 1975; Burdick,
220 1976; Kuznetsova et al., 2007).

221

222 Taken together, these results support a model, in which D1/HMGA1 bind their target
223 sequences (satellite DNA) on multiple chromosomes and bundle them into chromocenters, likely
224 via their multivalent DNA binding domains (multiple AT-hooks) (Figure 6E).

225

226 **Discussion**

227 The function of chromocenters, as well as that of satellite DNA, has remained enigmatic,
228 even though cytological association of pericentromeric satellite DNA into chromocenters was
229 identified almost 50 years ago (Jones, 1970; Pardue and Gall, 1970). Pericentromeric
230 heterochromatin has most often been studied and discussed in the context of how to maintain its
231 heterochromatic, repressed nature (Nishibuchi and Déjardin, 2017), based on the assumption that
232 the underlying sequences are mostly selfish, which have negative phenotypic consequences when
233 derepressed in cells (Zeller and Gasser, 2017).

234

235 Although satellite DNA's function has been speculated and implicated in several
236 examples (Yunis and Yasmineh, 1971; Bonaccorsi et al., 1990; Dernburg et al., 1996; Menon et
237 al., 2014), the non-coding nature and lack of conservation in repeat sequence among closely
238 related species led to the idea that they are mostly junk DNA, serving no essential function
239 (Walker, 1971; Doolittle and Sapienza, 1980). Instead, we propose that satellite DNA is a critical
240 constituent of eukaryotic chromosomes to ensure encapsulation of all chromosomes in interphase
241 nucleus. Our results may also explain why the sequences of pericentromeric satellite DNA are so
242 divergent among closely related species, a contributing factor that led to their dismissal as junk.
243 Based on our model that pericentromeric satellite DNA serves as a platform for generating
244 heterologous chromosome association to form chromocenters, the essential feature of satellite
245 DNA is that they are bound by protein(s) capable of bundling multiple DNA strands. If so, the
246 underlying sequence does not have to be conserved. Instead, the binding of satellite DNA by a
247 chromocenter bundling protein may be a critical feature of pericentromeric satellite DNAs.
248 Based on this idea, chromocenter bundling proteins and pericentromeric satellite DNA may be
249 co-evolving.

250

251 We observed perturbation of nuclear envelope integrity upon chromocenter disruption.
252 Understanding the mechanisms underlying perturbation of nuclear envelope integrity in *D1*
253 mutant awaits future investigation. Previous studies have documented that cytoskeletal forces are
254 transmitted to chromatin through nuclear envelope and external mechanical forces can cause
255 temporary nuclear envelope breaches (King et al., 2008; Denais et al., 2016; Hatch and Hetzer,
256 2016; Raab et al., 2016). Therefore, we speculate that chromosome bundling in the form of
257 chromocenter may help prevent cytoskeletal forces from shearing chromosomes and nuclear

envelope: when chromosomes are not bundled, cytoskeletal forces may be transmitted to individual chromosomes and associated nuclear envelope, resulting in shearing of nuclear envelope, disrupting its integrity.

In summary, our study provides the first evidence for a conserved function of pericentromeric satellite DNA and chromocenters. Our data suggest that the multi-AT hook proteins, D1 and HMGA1, play an evolutionarily conserved role in the formation of chromocenters, likely via their ability to bind and bundle satellite DNA from heterologous chromosomes. Heterologous chromosome association, mediated by chromocenter-binding proteins, may represent a third mode of chromosomal 'gluing' after meiotic homologous pairing and sister chromatid cohesion. Through heterologous association, the chromocenter plays a fundamental role in maintaining the full complement of the genome, which is divided into multiple chromosomes, into a single nucleus. This function of the chromocenter may be conserved in eukaryotic species that contain pericentromeric satellite DNA, thereby bringing about a signature characteristic of eukaryotic cells.

Acknowledgments:

We thank Cheng-Yu Lee, Scott Hawley, Stephen Weiss, Harry Mobley, Dave Bridges, Daniel Eitzman, Georg Krohne, Bloomington Drosophila Stock Center, Kyoto Stock Center, Developmental Studies Hybridoma Bank and Michigan Imaging Laboratory for reagents and resources. We thank the Yamashita lab members, Sue Hammoud, Ajit Joglekar, Puck Ohi, Dan Barbash, and Maurizio Gatti for discussion and comments on the manuscript. This research was supported by the Howard Hughes Medical Institute (Y.Y) and an American Heart Association postdoctoral fellowship (M.J). MJ and YY conceived the project, interpreted the data and wrote the manuscript. All authors contributed to conducting experiments and analyzing data.

Materials and Methods:

Key Resources Table

Reagent type (species) or	Designation	Source or reference	Identifiers	Additional information

resource				
Genetic Reagent (*D.melanogaster*)	D1^{EY05004}	Bloomington Drosophila Stock Center	ID_*BDSC:17340*	
Genetic Reagent (*D.melanogaster*)	Df(3R)BSC666	Bloomington Drosophila Stock Center	ID_*BDSC:26518*	
Genetic Reagent (*D.melanogaster*)	*UAS-Omi^{RNAi}*	Bloomington Drosophila Stock Center	ID_*BDSC:55165*	
Genetic Reagent (*D.melanogaster*)	*UAS-GFP-nls*	Bloomington Drosophila Stock Center	ID_*BDSC:4776*	
Genetic Reagent (*D.melanogaster*)	*UAS-GFP-ER-SR*	Bloomington Drosophila Stock Center	ID_*BDSC:59042*	
Genetic Reagent (*D.melanogaster*)	*D1^{LL03310}*	Kyoto Stock Center	ID_*DGRC:140754*	
Genetic Reagent (*D.melanogaster*)	Df31-GFP	Kyoto Stock Center	ID_*DGRC:110806*	
Genetic Reagent (*D.melanogaster*)	*nos-gal4*	PMID: 9501989		
Genetic Reagent (*D.melanogaster*)	hs-flp;nos-FRT-stop-FRT-gal4,UAS-GFP	PMID: 24465278		
Genetic Reagent (*D.melanogaster*)	*UAS-H2A-YFP*	PMID: 11146626		
Genetic Reagent (*D.melanogaster*)	*B1 LacO*	PMID: 12225662		
Genetic Reagent (*D.melanogaster*)	*mtrm^{126}+B*	PMID: 24478336		Gift of Dr. Scott Hawley
Recombinant DNA Reagent	*pUASt-GFP-attB*	PMID: 24465278		
Recombinant DNA Reagent	*pUASt-GFP-D1-attB*	This Paper		
Recombinant DNA Reagent	*pUASt-GFP-LacI-D1-attB*	This Paper		
Recombinant DNA Reagent	*pCDNA3*			Gift of Dr. Cheng-Yu Lee
Cell Line	MOVAS			Gift of Dr. Daniel Eitzman
Cell Line	C2C12			Gift of Dr. David Bridges
Cell Line	RAW264.7			Gift of Dr. Harry Mobley
Cell Line	C3H10T1/2			Gift of Dr. Stephen Weiss
siRNA	ON-TARGET plus Mouse HMGA1 siRNA SMARTpool	Dharmacon/GE Healthcare	ID_*Dharmacon: L-049293-01*	
siRNA	ON-TARGET plus Non-targeting pool	Dharmacon/GE Healthcare	ID_*Dharmacon: L-001810-10*	
Antibody	anti-Vasa	Santa Cruz Biotechnology	ID_*SCB: d-26*	
Antibody	anti-H3K9 dimethyl	Abcam	ID_*abcam: ab32521*	
Antibody	anti-Otefin			Gift of Dr. Georg Krohne
Antibody	anti-D1	This Paper		Peptide - CDGENDANDGYVSDNYNDSESVAA
Antibody	anti-LaminDm$_0$	Developmental Studies Hybridoma Bank	ID_*DSHB: ADL84.12*	
Antibody	anti-γ-H2Av	Developmental Studies Hybridoma Bank	ID_*DSHB: UNC93-5.2.1*	
Antibody	Phalloidin-Alexa546	ThermoFisher	ID_*ThermoFisher: a22283*	
Antibody	anti-HMGA1	Abcam	ID_*abcam: ab129153*	
Antibody	anti-LaminB (C20)	Santa Cruz Biotechnology	ID_*SCB: 2616*	

Antibody	anti-α-tubulin	Developmental Studies Hybridoma Bank	ID_*DSHB: 4.3*	
Antibody	anti-γ-H2Ax S139	Cell Signaling Technologies	ID_*CST: 2577*	

285

286 **Fly husbandry and strains.** All fly stocks were raised on standard Bloomington medium at
287 25°C. The following fly stocks were used: *D1*^{EY05004}(BDSC17340), Df(3R)BSC666
288 (BDSC26518), *UAS-Omi*^{RNAi} (BDSC55165), *UAS-GFP-nls* (BDSC4776) and *UAS-GFP-ER-SR*
289 (BDSC59042) were obtained from the Bloomington *Drosophila* stock center. *D1*^{LL03310}
290 (DGRC140754) and Df31-GFP (DGRC110806) were obtained from the Kyoto stock center. *nos-*
291 *gal4*(Van Doren et al., 1998), *hs-flp;nos-FRT-stop-FRT-gal4,UAS-GFP* (Salzmann et al., 2013),
292 *UAS-H2A-YFP* (Bellaïche et al., 2001) and *B1 LacO* (Vazquez et al., 2002) have been previously
293 described. A stock containing B chromosomes, *mtrm*^{126}*+B* (Bauerly et al., 2014), was a kind gift
294 from Scott Hawley. Chromocenter disruption was scored in Drosophila testes by assessing
295 $\{AATAT\}_n$ morphology in GFP+ cells that were generated as follows in control (hs-flp; *nos-*
296 *FRT-stop-FRT-gal4,UAS-GFP)* and *D1* mutant (*hs-flp;nos-FRT-stop-FRT-gal4, UAS-*
297 *GFP*;*D1*^{LL03310}/*Df*) flies. Testes were dissected 24h following a 20 minute heat shock at 37°C.
298 Chromocenters were considered disrupted in *Drosophila* and mouse when satellite DNA adopted
299 thread-like morphology in interphase nuclei. Micronuclei were scored in 0-3d testes where early
300 germ cell chromosomes were labeled with H2A-YFP. The genotypes used were, control –
301 *nos>H2A-YFP* and D1 mutant – *nos>H2A-YFP*; *D1LL03310/Df.*

302

303 **Transgene construction.** For construction of *UAS-GFP-D1*, the *D1* ORF was PCR-amplified
304 from cDNA using the following primer pair, 5'-
305 GATCAGATCTATGGAGGAAGTTGCGGTAAAG-3' and 5'-
306 GATCCTCGAGTTAGGCAGCTACCGATTCGG-3'. The amplified fragment was subcloned
307 into the BglII and XhoI sites of *pUASt-EGFP-attB*(Salzmann et al., 2013) resulting in *UAS-*
308 *GFP-D1*. For *UAS-GFP-LacI-D1*, the *LacI* ORF (lacking 11 C-terminal residues) (Straight et al.,
309 1996) was synthesized using GeneArt (Thermofisher) and inserted into the BglII site of *UAS-*
310 *GFP-D1* resulting in *UAS-GFP-LacI-D1*. Transgenic flies were generated by PhiC31 integrase-
311 mediated transgenesis into the *attP40* site (BestGene). For expression of GFP and GFP-D1 in

312 mouse cells, *GFP* and *GFP-D1* was subcloned from *pUASt-EGFP-attB* into pCDNA3 (gift from
313 Cheng-Yu Lee) using EcoRI and XhoI sites.

314

315 **Cell lines.** Mouse MOVAS cells were obtained from Daniel Eitzman. Mouse C2C12 cells were
316 obtained from David Bridges. Mouse RAW264.7 cells were obtained from Dr. Harry Mobley.
317 Mouse C3H10T1/2 cells were obtained from Stephen Weiss. MOVAS, C2C12 and RAW264.7
318 cells were maintained in Dulbecco's minimal essential medium (DMEM) (Gibco) supplemented
319 with 10% fetal bovine serum (FBS). C3H10T1/2 cell line was maintained in alpha minimal
320 essential media (Gibco) supplemented with 10% fetal bovine serum. All cell lines used were
321 authenticated as mouse cells by the presence of mouse-specific satellite DNA as is shown
322 throughout the manuscript. Two major cell lines used in this study, C2C12 and MOVAS cells,
323 were treated with Plasmocin (Invivogen) prior to use as a precaution for mycoplasma infection.

324

325 **siRNA and Transfections.** RNA interference (RNAi) against HMGA1 was performed using
326 ON-TARGET plus Mouse HMGA1 siRNA SMARTpool (Dharmacon, L-049293-01) consisting
327 of the following target sequences, CCAUUUAGCCGCAGCCCGA,
328 AGGCAAACGGGCACCAACA, GGGCGCAGCAGACUGGUUA,
329 GUUCAUUCUUAGAUACCCA. ON-TARGET plus Non-targeting pool (Dharmacon, D-
330 001810-10) consisting of the following sequences, UGGUUUACAUGUCGACUAA,
331 UGGUUUACAUGUUGUGUGA, UGGUUUACAUGUUUUCUGA,
332 UGGUUUACAUGUUUUCCUA, was used as a negative control. siRNA transfections were
333 performed using DharmaFECT 4 reagent (Dharmacon) according to the manufacturer's protocol.
334 25nM of siControl and siHMGA1 were transfected using DharmaFECT 4 (Dharmacon)
335 according to the manufacturer’s protocol. Cells were fixed for immunostaining/*in situ*
336 hybridization 6 days post transfection. Transient transfection of GFP and GFP-D1 was
337 performed using Fugene HD (Roche) reagent according to the manufacturer’s protocol.

338

339 **Immunofluorescence staining and microscopy.** For *Drosophila* tissues, immunofluorescence
340 staining was performed as described previously (Cheng et al., 2008). Briefly, tissues were

341 dissected in PBS, transferred to 4% formaldehyde in PBS and fixed for 30 minutes. Testes were
342 then washed in PBS-T (PBS containing 0.1% Triton-X) for at least 60 minutes, followed by
343 incubation with primary antibody in 3% bovine serum albumin (BSA) in PBS-T at 4°C
344 overnight. Samples were washed for 60 minutes (three 20-minute washes) in PBS-T, incubated
345 with secondary antibody in 3% BSA in PBS-T at 4°C overnight, washed as above, and mounted
346 in VECTASHIELD with DAPI (Vector Labs). The following primary antibodies were used:
347 rabbit anti-vasa (1:200; d-26; Santa Cruz Biotechnology), rabbit anti-H3K9 dimethyl (1:200;
348 Abcam, ab32521), guinea pig anti-Otefin (gift from Georg Krohne, 1:400), chicken anti-Cid
349 (1:500, generated using the synthetic peptide CDGENDANDGYVSDNYNDSESVAA
350 (Covance)), mouse anti-LaminDm$_0$ (ADL84.12, 1:200, Developmental Studies Hybridoma
351 Bank), mouse anti-γ–H2Av (UNC93-5.2.1, 1:400, Developmental Studies Hybridoma Bank),
352 Phalloidin-Alexa546 (ThermoFisher, a22283, 1:200). Adherent mouse cells were fixed in 4%
353 formaldehyde in PBS for 20 minutes at room temperature on coverslips. Cells were
354 permeabilized in PBS-T for 5 minutes, rinsed 3 times with PBS, blocked using 3% BSA in PBS-
355 T for 30 minutes at room temperature and incubated with primary antibody diluted in 3% BSA in
356 PBS-T overnight at 4°C. Cells were then washed for 30 minutes (three 10-minute washes),
357 incubated with secondary antibody in 3% BSA in PBS-T for 2 hours at room temperature,
358 washed as above and mounted in VECTASHIELD with DAPI (Vector Labs). For nucleoplasmic
359 extraction, cells were incubated with CSK buffer (10mM PIPES pH7, 100mM NaCl, 300mM
360 sucrose, 3mM $MgCl_2$, 0.5% Triton X-100, 1mM PMSF) for 10 minutes at room temperature.
361 After CSK extraction, cells were washed with PBS and fixed and immunostained as above. The
362 following antibodies were used: rabbit anti-HMGA1 (1:400, Abcam, ab129153), goat anti-
363 LaminB (C-20) (1:20, Santa Cruz Biotechnology, sc-2616), mouse anti-α-tubulin (4.3, 1:100,
364 Developmental Studies Hybridoma Bank) and γ–H2Ax S139 (2577, 1:200, Cell Signaling
365 Technologies). Images were taken using a Leica TCS SP8 confocal microscope with 63x oil-
366 immersion objectives (NA=1.4). Deconvolution was performed when indicated using the
367 Hyvolution package from Leica. Images were processed using Adobe Photoshop software.

368

369 **Time-lapse live imaging.** Testes from newly eclosed flies were dissected into
370 Schneider's *Drosophila* medium containing 10% fetal bovine serum. The testis tips were placed

371 inside a sterile glass-bottom chamber and were mounted on a three-axis computer-controlled
372 piezoelectric stage. An inverted Leica TCS SP8 confocal microscope with a 63× oil immersion
373 objective (NA = 1.4) was used for imaging. For mouse live cell imaging, transfected cells were
374 seeded onto a sterile glass-bottom chamber coated with poly-lysine. Cells were incubated with
375 Hoechst 33342 for 10 minutes, rinsed with PBS and fresh medium was added to the chamber.
376 Cells were imaged using a stage-top Tokai-Hit incubator that was mounted on an inverted TCS
377 SP5 confocal microscope with a 63x oil immersion objective (NA = 1.4). All images were
378 processed using Adobe Photoshop software. Metrics used for quantification of live imaging were
379 total imaging duration (defined as number of cells x imaging duration), total budding duration
380 (defined as number of cells with micronuclei that formed by budding x time with budded
381 micronuclei).

382

383 **DNA fluorescence *in situ* hybridization.** Whole mount *Drosophila* testes were prepared as
384 described above, and optional immunofluorescence staining protocol was carried out first.
385 Subsequently, samples were post-fixed with 4% formaldehyde for 10 minutes and washed in
386 PBS-T for 30 minutes. Fixed samples were incubated with 2 mg/ml RNase A solution at 37°C
387 for 10 minutes, then washed with PBS-T + 1mM EDTA. Samples were washed in 2xSSC-T
388 (2xSSC containing 0.1% Tween-20) with increasing formamide concentrations (20%, 40% and
389 50%) for 15 minutes each followed by a final 30-minute wash in 50% formamide. Hybridization
390 buffer (50% formamide, 10% dextran sulfate, 2x SSC, 1mM EDTA, 1 μM probe) was added to
391 washed samples. Samples were denatured at 91°C for 2 minutes, then incubated overnight at
392 37°C. For mitotic chromosome spreads, testes and larval 3rd instar brains were squashed
393 according to previously described methods (Larracuente and Ferree, 2015). Briefly, tissue was
394 dissected into 0.5% sodium citrate for 5-10 minutes and fixed in 45% acetic acid/2.2%
395 formaldehyde for 4-5 minutes. Fixed tissues were firmly squashed with a cover slip and slides
396 were submerged in liquid nitrogen until bubbling ceased. Coverslips were then removed with a
397 razor blade and slides were dehydrated in 100% ethanol for at least 5 minutes. After drying,
398 hybridization mix (50% formamide, 2x SSC, 10% dextran sulfate, 100 ng of each probe) was
399 applied directly to the slide, samples were heat denatured at 95°C for 5 minutes and allowed to
400 hybridize overnight at room temperature. Following hybridization, slides were washed 3 times
401 for 15 minutes in 0.2X SSC and mounted with VECTASHIELD with DAPI (Vector Labs). For

402 the *in situ* experiment described in Figure 4j-m, testes were dissected into PBS and fixed in 4%
403 formaldehyde for 4 minutes. Tips of fixed testes were firmly squashed with a cover slip and
404 slides were submerged in liquid nitrogen until bubbling ceased. Coverslips were removed with a
405 razor blade and slides were subjected to 5-minute washes in 2XSSC and 2XSSC with 0.1%
406 Tween-20. The samples were denatured in freshly made 0.07N NaOH for 5 minutes, rinsed in
407 2X SSC. Hybridization mix (50% formamide, 2x SSC, 10% dextran sulfate, 100 ng of each
408 probe) was added directly to the slide and allowed to hybridize overnight at room temperature.
409 Following hybridization, slides were washed 3 times for 15 minutes in 0.2X SSC and mounted
410 with VECTASHIELD with DAPI (Vector Labs). The following probes were used for *Drosophila*
411 in situ hybridization: $\{AATAT\}_6$, $\{AAGAG\}_6$, IGS and have been previously described
412 (Jagannathan et al., 2017). LacO probe - 5'-Cy5-
413 CCACAAATTGTTATCCGCTCACAATTCCAC-3'. For interphase mouse cells, optional
414 immunostaining was carried out as above. Subsequently, samples were post-fixed with 4%
415 formaldehyde in PBS for 10 minutes and rinsed three times in PBS. Post-fixed cells were
416 incubated with 0.1 mg/ml RNase A solution at 37°C for 1 hour, rinsed three times in PBS and
417 denatured in 1.9M HCl for 30 minutes. After three rinses in ice-cold PBS, hybridization mix (2X
418 SSC, 60% formamide, 5µg/ml salmon sperm DNA and 500nM probe) was added to the samples
419 and incubated overnight at room temperature. Following hybridization, coverslips were washed 3
420 times for 15 minutes in 2X SSC and mounted with VECTASHIELD with DAPI (Vector Labs).
421 For mouse mitotic cells, chromosomes were spread on slides as previously described.
422 Subsequently, chromosomes were denatured in 70% formamide in 2XSSC for 1.5 minutes at
423 70°C, dehydrated in 100% ethanol and hybridization mix (2X SSC, 60% formamide, 5µg/ml
424 salmon sperm DNA and 500nM probe) was added directly to the slide and incubated overnight at
425 room temperature. Following hybridization, slides were washed 3 times for 15 minutes in 2X
426 SSC and mounted with VECTASHIELD with DAPI (Vector Labs). The following probe was
427 used: Major satellite - 5'-Cy3-GGAAAATTTAGAAATGTCCACTG-3'.

428

429

430 **References:**

431 Aulner, N., Monod, C., Mandicourt, G., Jullien, D., Cuvier, O., Sall, A., Janssen, S., Laemmli,
432 U.K., and E. Käs. 2002. The AT-hook protein D1 is essential for *Drosophila*
433 *melanogaster* development and is implicated in position-effect variegation. *Mol. Cell.*
434 *Biol*. 22(4):1218-1232. doi:10.1128/MCB.22.4.1218-1232.2002

435 Barton, L.J., S.R. Wilmington, M.J. Martin, H.M. Skopec, K.E. Lovander, B.S. Pinto, and P.K.
436 Geyer. 2014. Unique and shared functions of nuclear lamina LEM domain proteins in
437 Drosophila. *Genetics*. 197:653–665. doi:10.1534/genetics.114.162941.

438 Bauerly, E., S.E. Hughes, D.R. Vietti, D.E. Miller, W. McDowell, and R.S. Hawley. 2014.
439 Discovery of supernumerary B chromosomes in Drosophila melanogaster. *Genetics*.
440 196:1007–16. doi:10.1534/genetics.113.160556.

441 Bellaïche, Y., M. Gho, J.A. Kaltschmidt, A.H. Brand, and F. Schweisguth. 2001. Frizzled
442 regulates localization of cell-fate determinants and mitotic spindle rotation during
443 asymmetric cell division. *Nat. Cell Biol.* 3:50–7. doi:10.1038/35050558.

444 Bonaccorsi, S., M. Gatti, C. Pisano, and A. Lohe. 1990. Transcription of a satellite DNA on two
445 Y chromosome loops of Drosophila melanogaster. *Chromosoma*. 99:260–6.
446 doi:10.1007/BF01731701.

447 Bulut-Karslioglu, A., V. Perrera, M. Scaranaro, I.A. de la Rosa-Velazquez, S. van de Nobelen,
448 N. Shukeir, J. Popow, B. Gerle, S. Opravil, M. Pagani, S. Meidhof, T. Brabletz, T.
449 Manke, M. Lachner, and T. Jenuwein. 2012. A transcription factor-based mechanism for
450 mouse heterochromatin formation. *Nat. Struct. Mol. Biol.* 19:1023–30.
451 doi:10.1038/nsmb.2382.

452 Burdick, A.B. 1976. Somatic cell chromosome interconnections in trypan preparations of
453 Chinese hamster testicular cells. *Exp. Cell Res.* 99:425–8.

454 Cheng, J., N. Türkel, N. Hemati, M.T. Fuller, A.J. Hunt, and Y.M. Yamashita. 2008. Centrosome
455 misorientation reduces stem cell division during ageing. *Nature*. 456:599–604.
456 doi:10.1038/nature07386.

457 Crasta, K., N.J. Ganem, R. Dagher, A.B. Lantermann, E.V. Ivanova, Y. Pan, L. Nezi, A.
458 Protopopov, D. Chowdhury, and D. Pellman. 2012. DNA breaks and chromosome
459 pulverization from errors in mitosis. *Nature*. 482:53–8. doi:10.1038/nature10802.

460 Denais, C.M., R.M. Gilbert, P. Isermann, A.L. McGregor, M. te Lindert, B. Weigelin, P.M.

461 Davidson, P. Friedl, K. Wolf, and J. Lammerding. 2016. Nuclear envelope rupture and
462 repair during cancer cell migration. *Science*. 352:353–8. doi:10.1126/science.aad7297.
463 Dernburg, A.F., J.W. Sedat, and R.S. Hawley. 1996. Direct evidence of a role for
464 heterochromatin in meiotic chromosome segregation. *Cell*. 86:135–46.
465 Doolittle, W.F., and C. Sapienza. 1980. Selfish genes, the phenotype paradigm and genome
466 evolution. *Nature*. 284:601–3.
467 Doren, M. Van, A.L. Williamson, and R. Lehmann. 1998. Regulation of zygotic gene expression
468 in Drosophila primordial germ cells. *Curr. Biol.* 8:243–6.
469 Dorn, G.W., C.F. Clark, W.H. Eschenbacher, M.-Y.Y. Kang, J.T. Engelhard, S.J. Warner, S.J.
470 Matkovich, and C.C. Jowdy. 2011. MARF and Opa1 control mitochondrial and cardiac
471 function in Drosophila. *Circ. Res.* 108:12–7. doi:10.1161/CIRCRESAHA.110.236745.
472 Fransz, P., J.H. De Jong, M. Lysak, M.R. Castiglione, and I. Schubert. 2002. Interphase
473 chromosomes in Arabidopsis are organized as well defined chromocenters from which
474 euchromatin loops emanate. *Proc. Natl. Acad. Sci. U.S.A.* 99:14584–9.
475 doi:10.1073/pnas.212325299.
476 Gall, J.G., Cohen, E.H. and Polan, M.L. 1971. Reptitive DNA sequences in drosophila.
477 *Chromosoma*. 33:319-344
478 Goodwin, G.H., C. Sanders, and E.W. Johns. 1973. A new group of chromatin-associated
479 proteins with a high content of acidic and basic amino acids. *Eur. J. Biochem.* 38:14–9.
480 Guenatri, M., D. Bailly, C. Maison, and G. Almouzni. 2004. Mouse centric and pericentric
481 satellite repeats form distinct functional heterochromatin. *J. Cell Biol.* 166:493–505.
482 doi:10.1083/jcb.200403109.
483 Hahn, M., S. Dambacher, S. Dulev, A. Kuznetsova, S. Eck, S. Worz, D. Sadic, M. Schulte, J.
484 Mallm, A. Maiser, P. Debs, H. Melchner, H. Leonhardt, L. Schermelleh, K. Rohr, K.
485 Rippe, Z. Storchova, and G. Schotta. 2013. Suv4-20h2 mediates chromatin compaction
486 and is important for cohesin recruitment to heterochromatin. *Genes & Development*.
487 27:859872. doi:10.1101/gad.210377.112.
488 Hatch, E.M., A.H. Fischer, T.J. Deerinck, and M.W. Hetzer. 2013. Catastrophic nuclear envelope
489 collapse in cancer cell micronuclei. *Cell*. 154:47–60. doi:10.1016/j.cell.2013.06.007.
490 Hatch, E.M., and M.W. Hetzer. 2015. Chromothripsis. *Curr. Biol.* 25:R397–9.
491 doi:10.1016/j.cub.2015.02.033.

492 Hatch, E.M., and M.W. Hetzer. 2016. Nuclear envelope rupture is induced by actin-based
493 nucleus confnement. *J. Cell. Biol*. 215(1):27-36. doi:10.1083/jcb.201603053
494 Jagannathan, M., N. Warsinger-Pepe, G.J. Watase, and Y.M. Yamashita. 2017. Comparative
495 analysis of satellite DNA in the Drosophila melanogaster species complex. *G3*
496 *(Bethesda)*. 7:693–704. doi:10.1534/g3.116.035352.
497 Jones, K.W. 1970. Chromosomal and nuclear location of mouse satellite DNA in individual
498 cells. *Nature*. 7:912-915
499 Kuznetsova, I.S., N.I. Enukashvily, E.M. Noniashvili, A.N. Shatrova, N.D. Aksenov, V.V.
500 Zenin, A.P. Dyban, and O.I. Podgornaya. 2007. Evidence for the existence of satellite
501 DNA-containing connection between metaphase chromosomes. *J. Cell. Biochem.*
502 101:1046–61. doi:10.1002/jcb.21237.
503 King, M.C., Drivas, T.G. and G.Blobel. 2008. A network of nuclear envelope membrane proteins
504 linking centromeres to microtubules. *Cell.* 134(3):427-38. doi: 10.1016/j.cell.2008.06.022
505 Levinger, L., and A. Varshavsky. 1982a. Selective arrangement of ubiquitinated and D1 protein-
506 containing nucleosomes within the Drosophila genome. *Cell*. 28:375–85.
507 Levinger, L., and A. Varshavsky. 1982b. Protein D1 preferentially binds A + T-rich DNA in
508 vitro and is a component of Drosophila melanogaster nucleosomes containing A + T-rich
509 satellite DNA. *Proc. Natl. Acad. Sci. U.S.A.* 79:7152–6.
510 Lohe, A.R., Hilliker, A.J., and P.A. Roberts. 1993. Mapping simple repeated DNA sequences in
511 heterochromatin of *Drosophila melanogaster*. *Genetics*. 134:1149-1174
512 Lund, T., J. Holtlund, M. Fredriksen, and S.G. Laland. 1983. On the presence of two new high
513 mobility group-like proteins in HeLa S3 cells. *FEBS Lett.* 152:163–7.
514 Lyon, MF, and AG Searle. 1989. Genetic variants and strains of the laboratory mouse. Oxford
515 University Press, Oxford (England)
516 Menon, D.U., C. Coarfa, W. Xiao, P.H. Gunaratne, and V.H. Meller. 2014. siRNAs from an X-
517 linked satellite repeat promote X-chromosome recognition in Drosophila melanogaster.
518 *Proc. Natl. Acad. Sci. U.S.A.* 111:16460–5. doi:10.1073/pnas.1410534111.
519 Nishibuchi, G., and J. Déjardin. 2017. The molecular basis of the organization of repetitive
520 DNA-containing constitutive heterochromatin in mammals. *Chromosome Res.* 25:77–87.
521 doi:10.1007/s10577-016-9547-3.
522 Pardue, M.L., and J.G. Gall. 1970. Chromosomal localization of mouse satellite DNA. *Science*.

523 168:1356–8.
524 Peters, A.H., D. O'Carroll, H. Scherthan, K. Mechtler, S. Sauer, C. Schöfer, K.
525 Weipoltshammer, M. Pagani, M. Lachner, A. Kohlmaier, S. Opravil, M. Doyle, M.
526 Sibilia, and T. Jenuwein. 2001. Loss of the Suv39h histone methyltransferases impairs
527 mammalian heterochromatin and genome stability. *Cell.* 107:323–37.
528 Pinheiro, I., R. Margueron, N. Shukeir, M. Eisold, C. Fritzsch, F.M. Richter, G. Mittler, C.
529 Genoud, S. Goyama, M. Kurokawa, J. Son, D. Reinberg, M. Lachner, and T. Jenuwein.
530 2012. Prdm3 and Prdm16 are H3K9me1 methyltransferases required for mammalian
531 heterochromatin integrity. *Cell.* 150:948–60. doi:10.1016/j.cell.2012.06.048.
532 Probst, A.V., I. Okamoto, M. Casanova, F. El Marjou, P. Le Baccon, and G. Almouzni. 2010. A
533 strand-specific burst in transcription of pericentric satellites is required for chromocenter
534 formation and early mouse development. *Dev. Cell.* 19:625–38.
535 doi:10.1016/j.devcel.2010.09.002.
536 Raab, M., M. Gentili, H. de Belly, H.R. Thiam, P. Vargas, A.J. Jimenez, F. Lautenschlaeger, R.
537 Voituriez, A.M. Lennon-Duménil, N. Manel, and M. Piel. 2016. ESCRT III repairs
538 nuclear envelope ruptures during cell migration to limit DNA damage and cell death.
539 *Science*. 352:359–62. doi:10.1126/science.aad7611.
540 Radic, M.Z., M. Saghbini, T.S. Elton, R. Reeves, and B.A. Hamkalo. 1992. Hoechst 33258,
541 distamycin A, and high mobility group protein I (HMG-I) compete for binding to mouse
542 satellite DNA. *Chromosoma.* 101:602–8.
543 Rodriguez Alfageme, C., G.T. Rudkin, and L.H. Cohen. 1980. Isolation, properties and cellular
544 distribution of D1, a chromosomal protein of Drosophila. *Chromosoma.* 78:1–31.
545 Salzmann, V., M. Inaba, J. Cheng, and Y.M. Yamashita. 2013. Lineage tracing quantification
546 reveals symmetric stem cell division in Drosophila male germline stem cells. *Cell Mol*
547 *Bioeng*. 6:441–448. doi:10.1007/s12195-013-0295-6.
548 Straight, A.F., A.S. Belmont, C.C. Robinett, and A.W. Murray. 1996. GFP tagging of budding
549 yeast chromosomes reveals that protein-protein interactions can mediate sister chromatid
550 cohesion. *Curr. Biol.* 6:1599–608.
551 Strauss, F., and A. Varshavsky. 1984. A protein binds to a satellite DNA repeat at three specific
552 sites that would be brought into mutual proximity by DNA folding in the nucleosome.
553 *Cell.* 37:889–901.

554 Sun, X., H.D. Le, J.M. Wahlstrom, and G.H. Karpen. 2003. Sequence analysis of a functional
555 Drosophila centromere. *Genome Res.* 13:182–94. doi:10.1101/gr.681703.
556 Sun, X., J. Wahlstrom, and G. Karpen. 1997. Molecular structure of a functional Drosophila
557 centromere. *Cell.* 91:1007–19.
558 Takayama, S. 1975. Interchromosomal connectives in squash preparations of L cells. *Exp. Cell*
559 *Res.* 91:408–12.
560 Vazquez, J., A.S. Belmont, and J.W. Sedat. 2002. The dynamics of homologous chromosome
561 pairing during male Drosophila meiosis. *Curr. Biol.* 12:1473–83.
562 Vogel, B., A. Löschberger, M. Sauer, and R. Hock. 2011. Cross-linking of DNA through
563 HMGA1 suggests a DNA scaffold. *Nucleic Acids Res.* 39:7124–33.
564 doi:10.1093/nar/gkr396.
565 Walker, P.M. 1971. Origin of satellite DNA. *Nature*. 229:306–8.
566 Willard, H.F. 1990. Centromeres of mammalian chromosomes. *Trends Genet.* 6:410–6.
567 Yacobi-Sharon, K., Y. Namdar, and E. Arama. 2013. Alternative germ cell death pathway in
568 Drosophila involves HtrA2/Omi, lysosomes, and a caspase-9 counterpart. *Dev. Cell.*
569 25:29–42. doi:10.1016/j.devcel.2013.02.002.
570 Yunis, J.J., and W.G. Yasmineh. 1971. Heterochromatin, satellite DNA, and cell function.
571 Structural DNA of eucaryotes may support and protect genes and aid in speciation.
572 *Science*. 174:1200–9. doi:10.1126/science.174.4015.1200.
573 Zeller, P., and S.M. Gasser. 2017. The Importance of Satellite Sequence Repression for Genome
574 Stability. *Cold Spring Harb. Symp. Quant. Biol.* doi:10.1101/sqb.2017.82.033662.
575 Zeller, P., J. Padeken, R. van Schendel, V. Kalck, M. Tijsterman, and S.M. Gasser. 2016.
576 Histone H3K9 methylation is dispensable for Caenorhabditis elegans development but
577 suppresses RNA:DNA hybrid-associated repeat instability. *Nat. Genet.* 48:1385–1395.
578 doi:10.1038/ng.3672.
579 Zhang, C.-Z.Z., A. Spektor, H. Cornils, J.M. Francis, E.K. Jackson, S. Liu, M. Meyerson, and D.
580 Pellman. 2015. Chromothripsis from DNA damage in micronuclei. *Nature*. 522:179–84.
581 doi:10.1038/nature14493.
582 Zhu, Q., G.M. Pao, A.M. Huynh, H. Suh, N. Tonnu, P.M. Nederlof, F.H. Gage, and I.M. Verma.
583 2011. BRCA1 tumour suppression occurs via heterochromatin-mediated silencing.
584 *Nature*. 477:179–84. doi:10.1038/nature10371.

585

586

587 **Figure legends**

588 **Figure 1. Multi-AT-hook proteins, D1 and HMGA1, are required for chromocenter**
589 **formation in *Drosophila* and mouse cells.**
590 (A) Schematic of pericentromeric heterochromatin being organized into the chromocenter. (B)
591 FISH against $\{AATAT\}_n$ satellite (red) on the *Drosophila* neuroblast mitotic chromosomes co-
592 stained with DAPI (blue) indicating the location of $\{AATAT\}_n$ in the *Drosophila* genome. (C)
593 FISH against $\{AATAT\}_n$ satellite (red) in spermatogonial cells immunostained for H3K9me2
594 (blue) and D1 (green). Dotted lines indicate nucleus. Bars: 5µm. (D) *Drosophila* neuroblast
595 mitotic chromosomes stained for D1 (green), phospho-histone H3 Serine 10 (pH3-S10) (blue)
596 and Cid/CENP-A (red). (E-G) FISH against the mouse major satellite (green) on C2C12 mitotic
597 chromosomes co-stained with DAPI (blue) (E), in interphase MOVAS cells co-stained for DAPI
598 (blue) and HMGA1 (red) (F) and in MOVAS cells expressing GFP-D1 (blue) stained for
599 HMGA1 (red) (G). (H, I) FISH against $\{AATAT\}_n$ satellite (red) in control ($D1^{LL03310}$/+) (H) and
600 $D1^{LL03310}/Df$ (I) spermatogonial cells stained for DAPI (blue) and Vasa (green). (J)
601 Quantification of spermatogonial cells with disrupted chromocenters (+/+ control n=117,
602 $D1^{LL03310}/Df$ n=89) from three independent experiments. P value from student's t-test is shown.
603 Error bars: SD. (K, L) FISH against the major satellite (green) in siControl (K) and siHMGA1
604 (L) transfected MOVAS cells co-stained with DAPI (blue). (M) Quantification of cells with
605 disrupted chromocenters from siControl (n=304) and siHMGA1 (n=329) from three independent
606 experiments.

607

608 **Figure 1- figure supplement 1. AT-hook containing proteins, *Drosophila* D1 and mouse**
609 **HMGA1, localize to chromocenters in various mouse cell types.**
610 (A, B) FISH against the mouse major satellite (red) in C2C12 (A) and RAW 264.7 (B) cells
611 stained for HMGA1 (green) and DAPI (blue). (C, D) Colocalization of GFP-D1 (green) with
612 DAPI-dense chromocenters in C2C12 (C) and RAW 264.7(D) cells. DAPI (red). Scale bars:
613 5µm.

614

615 **Figure 1- figure supplement 2. *Drosophila* D1 and mouse HMGA1 are required for**
616 **chromocenter formation.**

617 (A-C) Testes from control (+/*Df*) (A) and two *D1* mutant ($D1^{LL03310}$/*Df* (B)and $D1^{EY05004}$/*Df* (C))
618 flies were stained for DAPI (blue), Phalloidin (red) and D1 (green). Asterisks indicate the apical
619 tip of the testis. Bars: 5μm. (D, E) FISH against $\{AATAT\}_n$ (red) in control ($D1^{EY05004}$/+) (D)
620 and $D1^{EY05004}$/*Df* (E) spermatogonial cells stained for DAPI (blue) and Vasa (green). Bars:
621 2.5μm. (F, G) FISH against $\{AATAT\}_n$ (red) in control ($D1^{LL03310}$/+) (F) and $D1^{LL03310}$/*Df* (G)
622 spermatocytes stained for DAPI (blue) and Vasa (green). (H, I) FISH against $\{AATAT\}_n$ (red) in
623 control ($D1^{LL03310}$/+) (H) and $D1^{LL03310}$/*Df* (I) accessory gland cells stained for DAPI (blue). Bars:
624 5μm. (J, K) FISH against the major satellite (green) in siControl (J) and siHMGA1 transfected
625 (K) C2C12 cells. Dotted lines indicate nucleus. (L) Quantification of cells with disrupted
626 chromocenters in siControl (n=304) and siHMGA1 (n=298) transfected C2C12 cells from three
627 independent experiments. P value from student's t-test is shown. Error bars: SD.
628
629 **Figure 2. D1/HMGA1 loss of function results in micronuclei formation, and defective**
630 **nuclear envelope integrity.**
631 (A, B) Control ($D1^{LL03310}$/+) (A) and $D1^{LL03310}$/*Df* mutant (B) spermatogonial cells stained for
632 DAPI (red), Vasa (blue) and $LaminDm_0$ (green). Arrow indicates micronucleus. Bars: 5μm. (C)
633 Quantification of micronuclei containing cells from +/+ control (n=269) and $D1^{LL03310}$/*Df*
634 (n=334) from three independent experiments. P value from student's t-test is shown. Error bars:
635 SD. (D, E) siControl (D) and siHMGA1 transfected (E) MOVAS cells stained for DAPI (blue),
636 HMGA1 (red) and Lamin (green). Arrow indicates micronucleus. (F) Quantification of
637 micronuclei containing cells in siControl (n=518) and siHMGA1 (n=588) transfected cells from
638 four independent experiments. (G, H) Control ($D1^{LL03310}$/+) (G) and $D1^{LL03310}$/*Df* (H)
639 spermatogonia expressing nls-GFP (green) stained for Vasa (blue) and $LaminDm_0$ (red). nlsGFP
640 was observed in cytoplasm in $D1^{LL03310}$/*Df* spermatogonia. (I) Quantification of spermatogonia
641 with cytoplasmic GFP (>1μm exclusions or pan-cytoplasmic) in $D1^{LL03310}$/+ (n=810) and
642 $D1^{LL03310}$/*Df* (n=780) testes from two independent experiments. (J, K) $D1^{LL03310}$/+ (J) and
643 $D1^{LL03310}$/*Df* (K) spermatogonia expressing ER-GFP marker (green) stained for Vasa (blue) and
644 $LaminDm_0$ (red). Arrowhead points to ER marker-positive micronucleus. Arrows point to site of
645 weak nuclear $LaminDm_0$ staining. (L, M) Control ($D1^{LL03310}$/+) (L) and $D1^{LL03310}$/*Df* (M)
646 spermatogonia stained for Vasa (blue) and $LaminDm_0$ (green) and Otefin (red). Arrowhead

647 points to Otefin-containing micronucleus. Arrows point to site of weak nuclear $LaminDm_0$
648 staining.
649
650 **Figure 2 –figure supplement 1. Formation of micronuclei upon chromocenter disruption in**
651 **C3H10T1/2 and C2C12 mouse cells.**
652 (A, B) siControl (A) and siHMGA1 (B) transfected C3H10T1/2 cells stained for DAPI (blue),
653 HMGA1 (red) and LaminB (green). Arrowhead indicates micronuclei. Bars: 5μm. (C)
654 Quantification of micronuclei containing cells from siControl (n=291) and siHMGA1 (n=303)
655 transfected cells from three independent experiments. P value from student's t-test is shown.
656 Error bars are SD. (D, E) siControl (D) and siHMGA1 (E) transfected C2C12 cells stained for
657 DAPI (blue), HMGA1 (red) and LaminB (green). Arrowhead indicates micronuclei. Bars: 5μm.
658 (F) Quantification of micronuclei containing cells from siControl (n=953) and siHMGA1
659 (n=699) transfected cells from three independent experiments. P value from student's t-test is
660 shown. Error bars are SD.
661
662 **Figure 3. D1 mutation/HMGA1 depletion leads to an increase in DNA damage.**
663 (A, B) Control ($D1^{LL03310}$/+) (A) and $D1^{LL03310}$/*Df* (B) spermatogonia stained for DAPI (blue),
664 Vasa (green) and γ-H2Av (red). Dotted lines indicate nucleus and arrow points to DNA damage
665 in micronuclei. (C, D) siControl (C) and siHMGA1 (D) transfected MOVAS cells stained for
666 DAPI (blue), γ-H2Av (red) and $LaminDm_0$ (green). Arrow points to DNA damage in
667 micronuclei. (E) Quantification of γ-H2Av positive cells in $D1^{LL03310}$/+ (n=317) and $D1^{LL03310}$/Df
668 (n=242) spermatogonia from three independent experiments. (F) Quantification of cells
669 containing >6 γ-H2Ax foci in siControl (n=304) and siHMGA1 (n=309) transfected cells from
670 three independent experiments. (G, H) FISH against the rDNA intergenic spacer (IGS) (green),
671 $\{AATAT\}_n$ (red) and $\{AAGAG\}_n$ (blue) on chromosome spreads from meiotic spermatocytes
672 from control (*nos>Omi*^{RNAi}, n=27) and *D1* mutant (*nos>Omi* ^{RNAi}; $D1^{LL03310}$/*Df*, n=57) testes co-
673 stained for DAPI (grey). *Omi*^{RNAi} was used to block DNA damage-induced cell death.
674 Arrowheads point to chromosome breaks.
675
676 **Figure 3 –figure supplement 1. Chromocenter disruption results in germ cell death in**
677 **Drosophila in an Omi-dependent manner.**

678 (A, B) Representative images of 14-day-old control ($D1^{LL03310}$/+, n=18) and $D1^{LL03310}/Df$ (n=12)
679 testes stained for DAPI (blue) and the germ cell marker, Vasa (green). Asterisk indicates apical
680 tip. Bars: 25μm (C, D) Representative images of *D1* mutant testes ($D1^{LL03310}/Df$) without (C) and
681 with (D) germ cell death suppression by *Omi* knockdown ($nos>Omi^{RNAi}$), stained for DAPI
682 (blue), Vasa (green) and $LaminDm_0$ (red) at 7 days post eclosion. (E, F) Representative images
683 of control ($nos>Omi^{RNAi}$, $D1^{LL033010}$/+, n=10) and *D1* mutant ($nos>Omi^{RNAi}$; $D1^{LL03310}/Df$, n=13)
684 testes stained for DAPI (blue), Vasa (green) and γ-H2Av (red).
685

686 **Figure 4. D1/HMGA1 loss of function results in micronuclei formation due to nuclear**
687 **budding during interphase.**
688 (A, B) Time-lapse live imaging of control (+/+) (A) and $D1^{LL03310}/Df$ (B) spermatogonial cells
689 expressing Df31-GFP as a nuclear marker and H2Av-RFP as a DNA marker. (C, D) Time-lapse
690 live imaging of siControl (C) and siHMGA1 (D) MOVAS cells stained with Hoechst 33342.
691 Arrowheads indicate site of micronucleus budding. Time is indicated in mm:ss. Scale bars: 5μm.
692

693 **Figure 4-figure supplement 1. Micronuclei formation upon chromocenter disruption is not**
694 **a result of mitotic lagging chromosomes.**
695 (A, B) Examples of normal and lagging mitotic chromosomes in *Drosophila* spermatogonia
696 stained for Vasa (blue) and pH3-S10 (green). (C) Quantification of spermatogonia with lagging
697 chromosomes from control ($D1^{LL033010}$/+, n=43) and $D1^{LL03310}/Df$ (n=47) from three independent
698 experiments. P value from student's t test is shown. Error bars are SD. (D, E) Examples of
699 normal and lagging mitotic chromosomes in mouse cells stained for DAPI (red) and α-tubulin
700 (green). Bars: 5μm. (F) Quantification of mitotic cells with lagging chromosomes from siControl
701 (n=149) and siHMGA1 (n=174) transfected MOVAS cells from three independent experiments.
702 (G) Quantification of mitotic cells with lagging chromosomes from siControl (n=110) and
703 siHMGA1 (n=129) transfected C2C12 cells from three independent experiments.
704

705 **Figure 5. D1/HMGA1 bundles satellite DNA from heterologous chromosomes to form**
706 **chromocenter.**
707 (A, B) C2C12 cells expressing GFP only (blue) (A) or GFP-D1 (blue) (B) stained for DAPI
708 (red). Dotted lines indicate nucleus. (C) Quantification of chromocenter number relative to

709 expression level of GFP (n=29) or GFP-D1 (n=47). P value and R^2 value are indicated from
710 linear regression analysis. (D) FISH against LacO (red) and $\{AATAT\}_n$ (green) on mitotic
711 neuroblast chromosomes from the LacO strain stained for DAPI (blue), indicating the sites of
712 LacO insertion (arrows). (E, F) FISH against LacO (red) and $\{AATAT\}_n$ (green) in
713 spermatogonia expressing GFP-D1 (blue) (E) or GFP-LacI-D1 (blue) (F). Arrows indicate
714 location of LacO sequence. (G) AATAT-LacO distance (nm) in GFP-D1 (n=97) and GFP-LacI-
715 D1 (n=69) expressing spermatogonia. P value from student's t-test is shown. Error bars: SD. All
716 scale bars: 5μm.
717
718 **Figure 6. D1/HMGA1 and satellite DNA form chromatin threads that link chromosomes**.
719 (A) Deconvolution microscopy performed on *Drosophila* mitotic neuroblasts stained for D1
720 (cyan) and pH3-S10 (magenta). Arrows in magnified images indicate D1-positive thread
721 connecting two chromosomes. (B) Deconvolution microscopy performed on CSK-extracted
722 RAW 264.7 macrophages stained for HMGA1 (cyan) and DAPI (magenta). Arrows in magnified
723 images indicate HMGA1-positive thread connecting two chromosomes. (C) Deconvolution
724 microscopy performed on neuroblast mitotic chromosomes stained for DAPI (magenta) and
725 FISH against $\{AATAT\}_n$ (cyan) from a *Drosophila* strain containing AATAT-rich B
726 chromosomes (Bauerly et al., 2014). Dotted lines in magnified images indicate AATAT-positive
727 threads connecting heterologous chromosomes. (D) Deconvolution microscopy performed on
728 RAW 264.7 macrophages stained for DAPI (magenta) and FISH against major satellite (cyan).
729 Dotted lines in magnified images indicate major satellite-positive threads connecting two
730 chromosomes. (E) The model of chromosome bundling by D1/HMGA1 and satellite DNA.

Figure 1

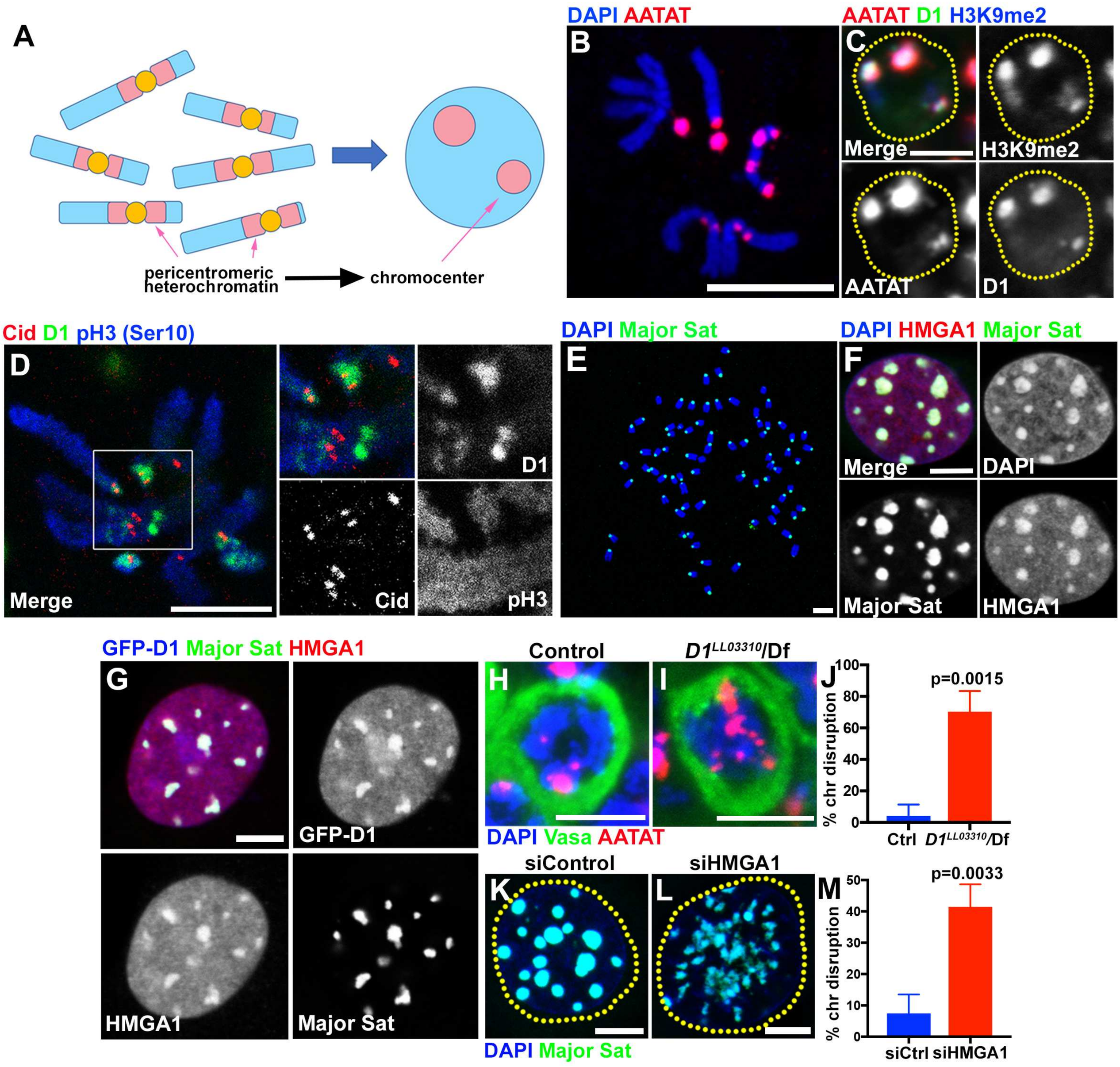
A
pericentromeric heterochromatin
chromocenter
DAPI AATAT
B
AATAT D1 H3K9me2
C
Merge
H3K9me2
AATAT
D1
Cid D1 pH3 (Ser10)
D
Merge
D1
Cid
pH3
DAPI Major Sat
E
DAPI HMGA1 Major Sat
F
Merge
DAPI
Major Sat
HMGA1
GFP-D1 Major Sat HMGA1
G
GFP-D1
HMGA1
Major Sat
Control
D1LL03310/Df
H
I
DAPI Vasa AATAT
J
p=0.0015
% chr disruption
100
80
60
40
20
0
Ctrl
D1LL03310/Df
siControl
siHMGA1
K
L
DAPI Major Sat
M
p=0.0033
% chr disruption
50
40
30
20
10
0
siCtrl
siHMGA1

Figure 2

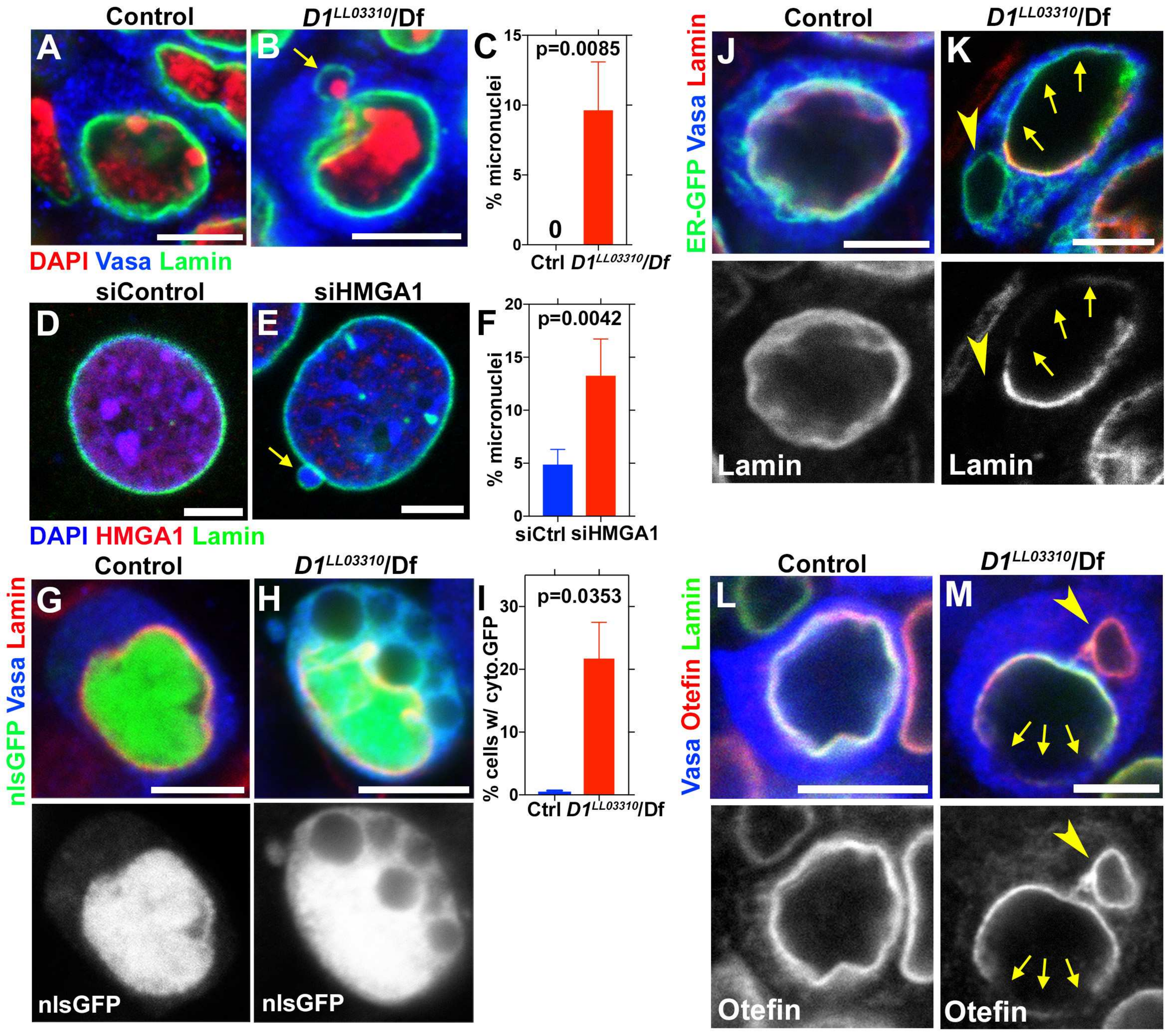
Control
D1LL03310/Df
A
B
C
p=0.0085
% micronuclei
0
Ctrl D1LL03310/Df
DAPI Vasa Lamin
siControl
siHMGA1
D
E
F
p=0.0042
% micronuclei
siCtrl siHMGA1
DAPI HMGA1 Lamin
Control
D1LL03310/Df
G
H
I
p=0.0353
% cells w/ cyto.GFP
Ctrl D1LL03310/Df
nlsGFP Vasa Lamin
nlsGFP
nlsGFP
Control
D1LL03310/Df
J
K
ER-GFP Vasa Lamin
Lamin
Lamin
Control
D1LL03310/Df
L
M
Vasa Otefin Lamin
Otefin
Otefin

Figure 3

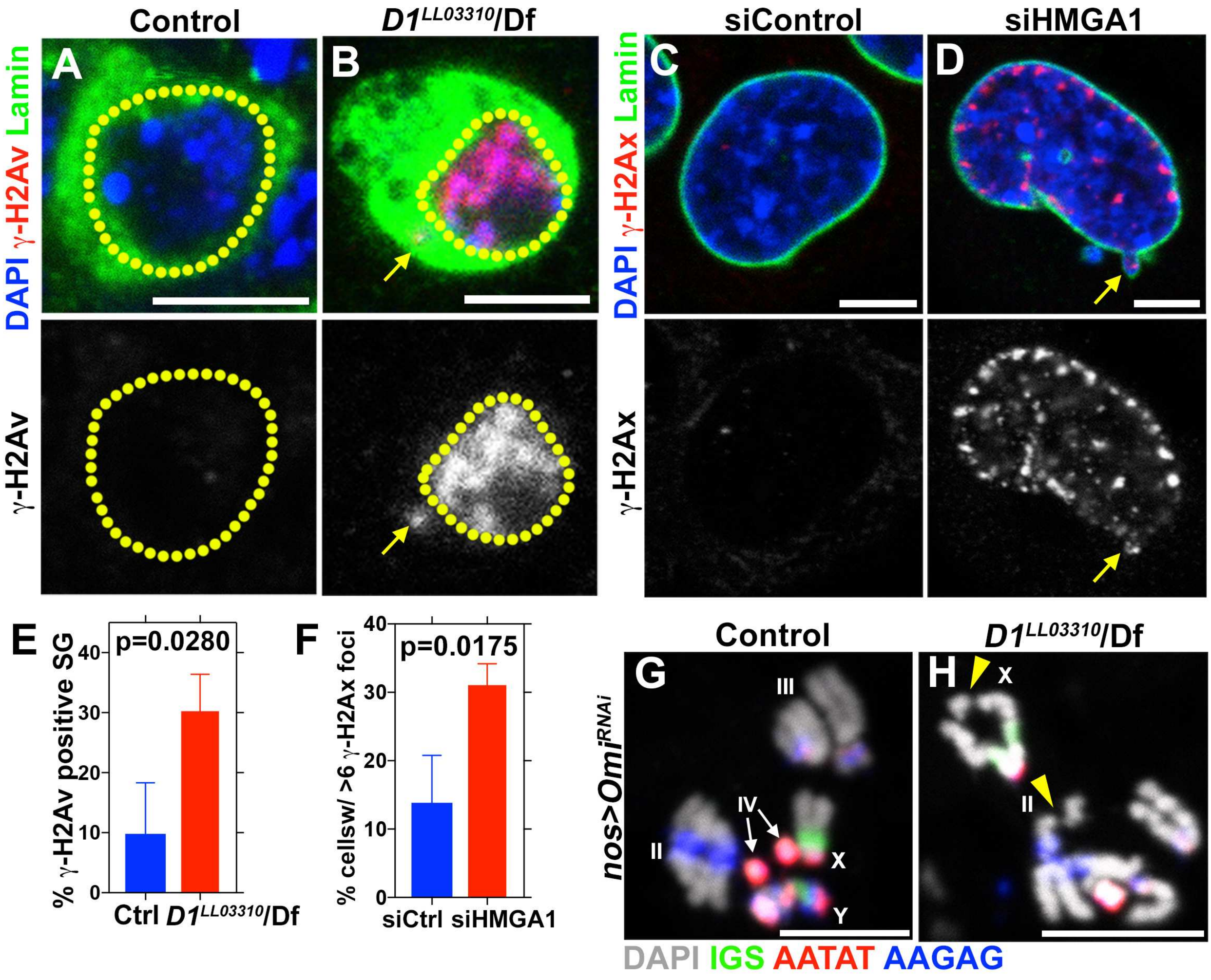
Control
D1LL03310/Df
siControl
siHMGA1
DAPI γ-H2Av Lamin
DAPI γ-H2Ax Lamin
γ-H2Av
γ-H2Ax
A
B
C
D
E
p=0.0280
% γ-H2Av positive SG
Ctrl D1LL03310/Df
F
p=0.0175
% cellsw/ >6 γ-H2Ax foci
siCtrl siHMGA1
Control
D1LL03310/Df
nos>OmiRNAi
G
H
III
IV
II
X
Y
DAPI IGS AATAT AAGAG

Figure 4

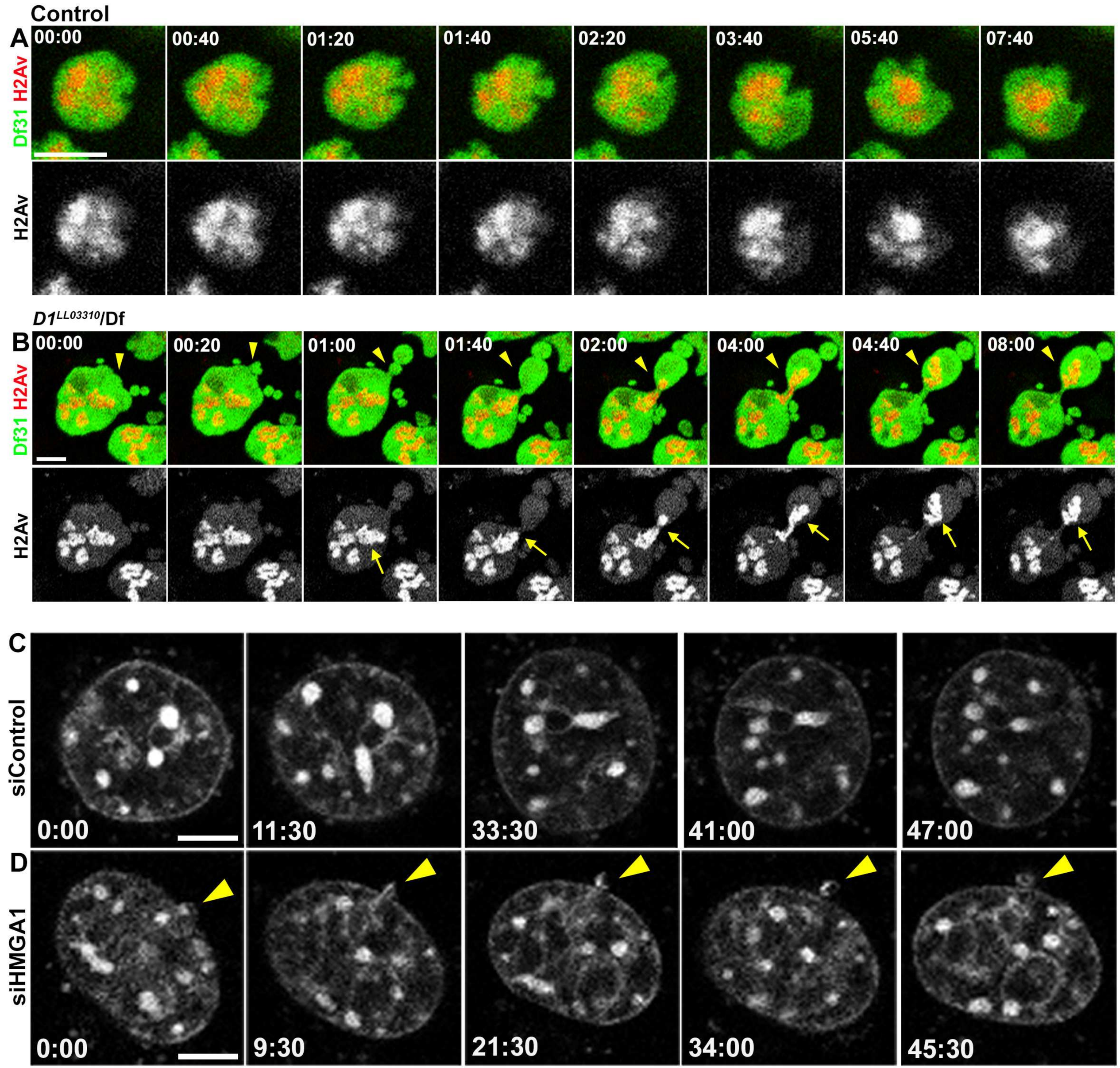
Control
A
Df31 H2Av
H2Av
00:00
00:40
01:20
01:40
02:20
03:40
05:40
07:40
D1LL03310/Df
B
Df31 H2Av
H2Av
00:00
00:20
01:00
01:40
02:00
04:00
04:40
08:00
C
siControl
0:00
11:30
33:30
41:00
47:00
D
siHMGA1
0:00
9:30
21:30
34:00
45:30

Figure 5

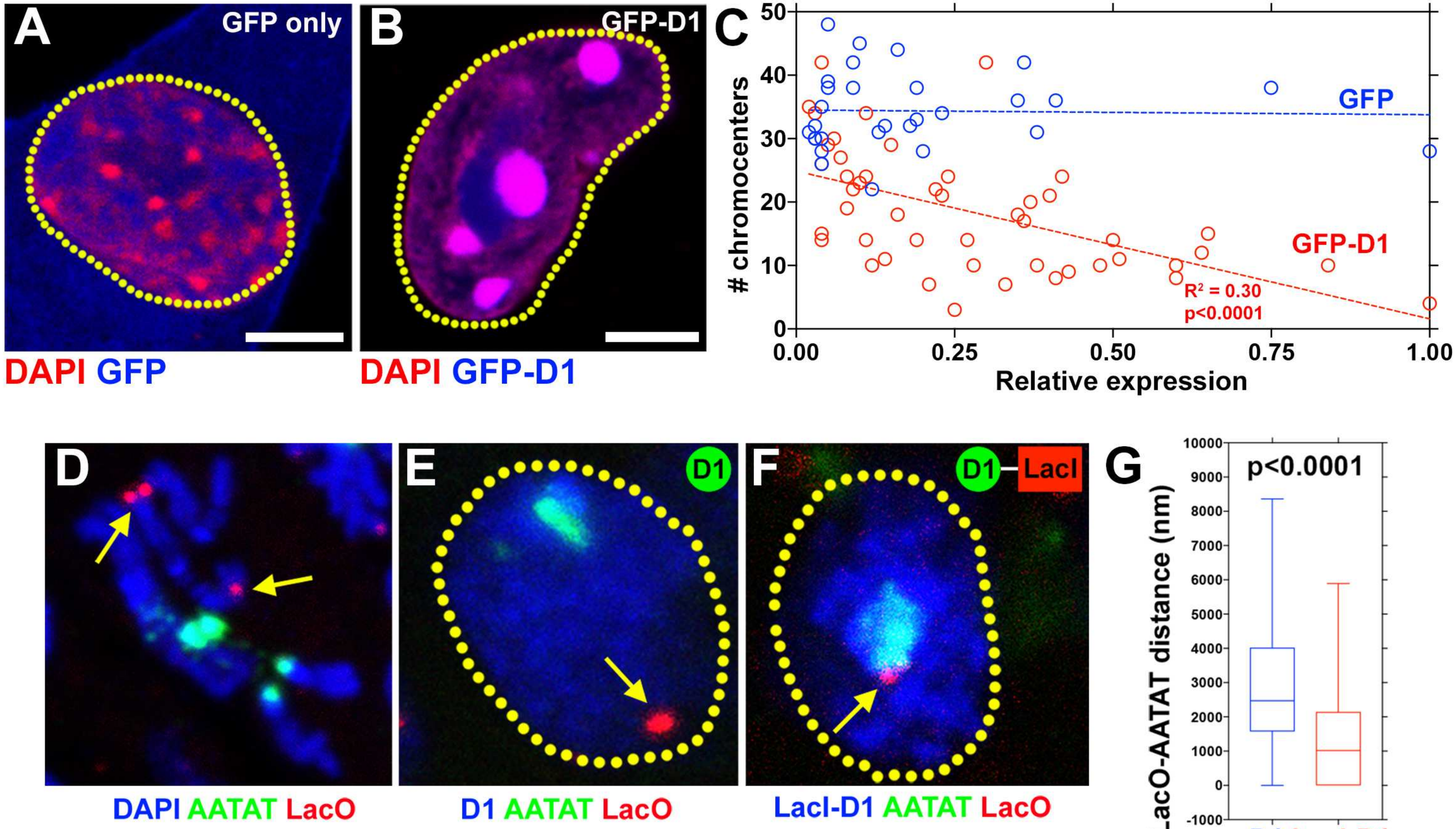
A
GFP only
DAPI GFP
B
GFP-D1
DAPI GFP-D1
C
chromocenters
Relative expression
GFP
GFP-D1
R² = 0.30
p<0.0001
0.00
0.25
0.50
0.75
1.00
0
10
20
30
40
50
D
DAPI AATAT LacO
E
D1
D1 AATAT LacO
F
D1
LacI
LacI-D1 AATAT LacO
G
p<0.0001
LacO-AATAT distance (nm)
-1000
0
1000
2000
3000
4000
5000
6000
7000
8000
9000
10000
D1
LacI-D1

Figure 6

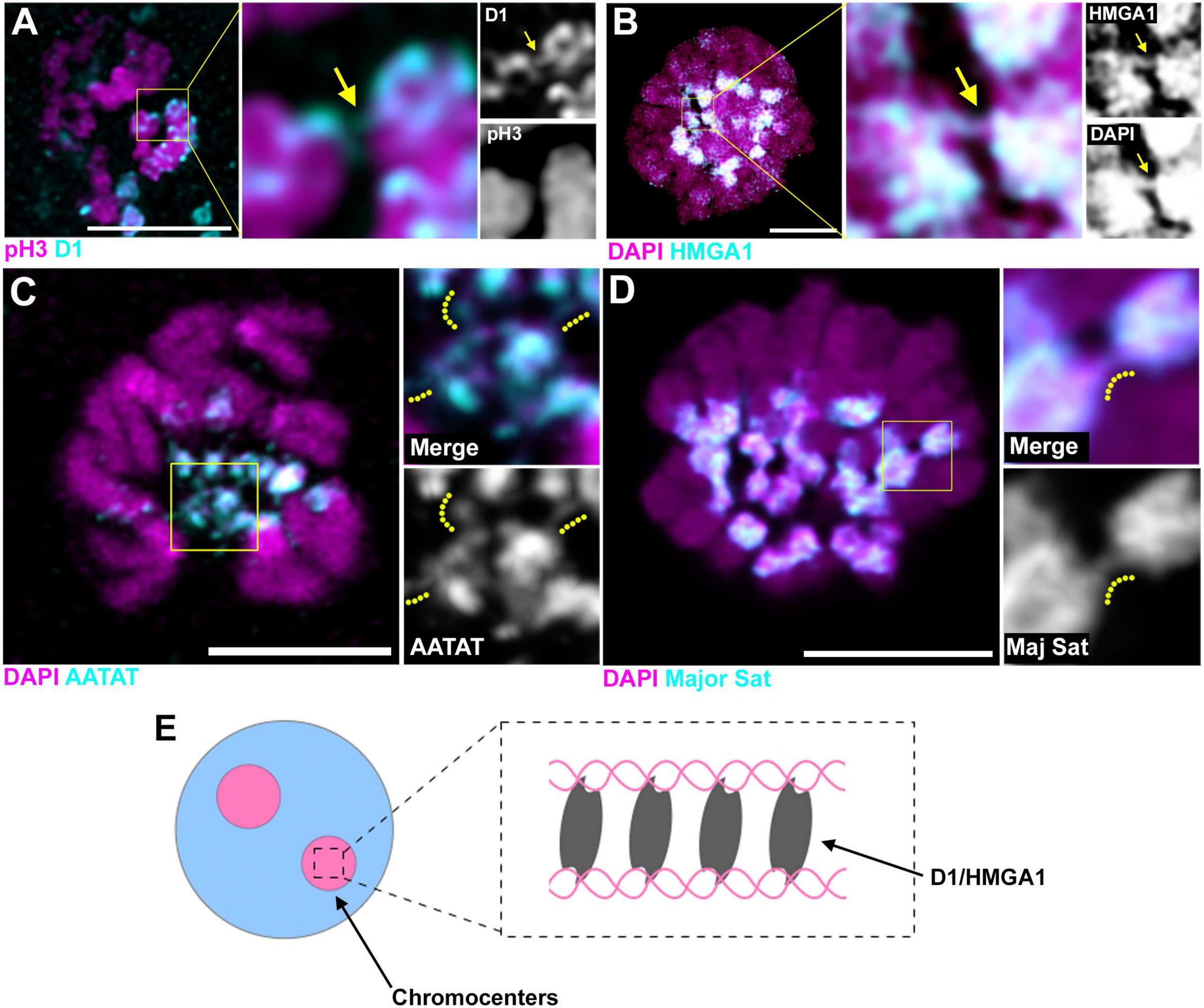
A
D1
pH3
pH3 D1
B
HMGA1
DAPI
DAPI HMGA1
C
Merge
AATAT
DAPI AATAT
D
Merge
Maj Sat
DAPI Major Sat
E
D1/HMGA1
Chromocenters

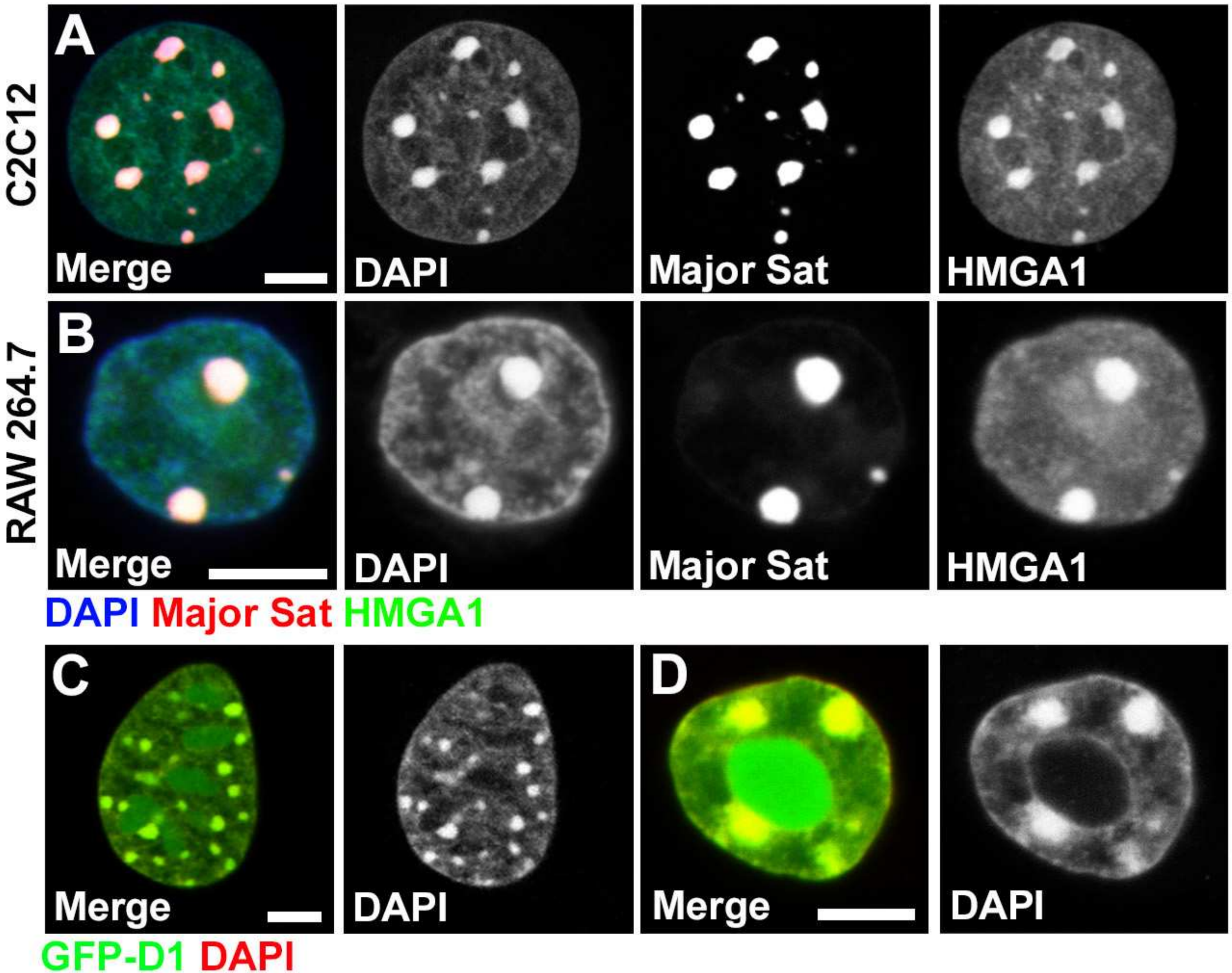
A
C2C12
Merge
DAPI
Major Sat
HMGA1
B
RAW 264.7
Merge
DAPI
Major Sat
HMGA1
DAPI Major Sat HMGA1
C
Merge
DAPI
D
Merge
DAPI
GFP-D1 DAPI

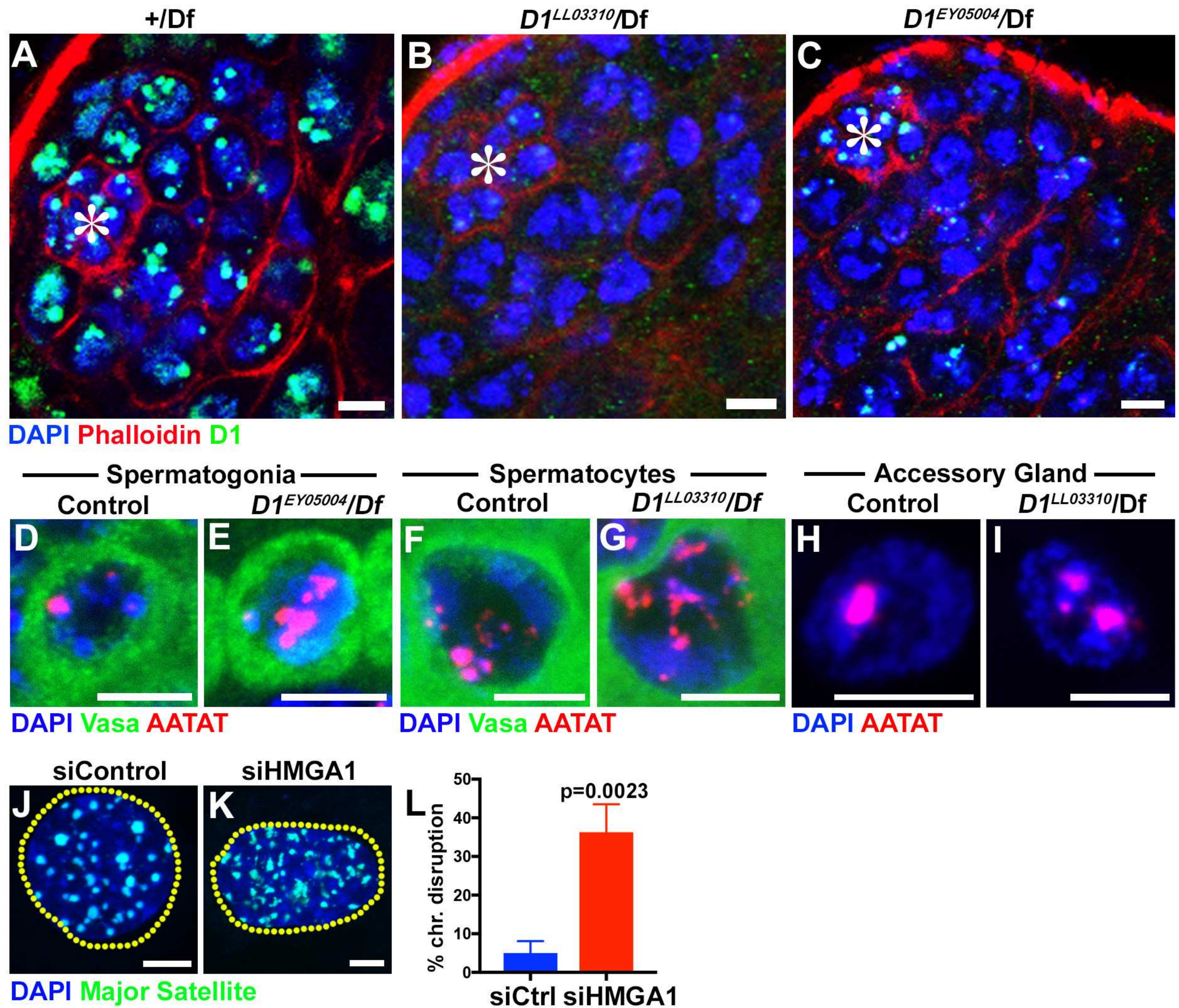
+/Df
D1LL03310/Df
D1EY05004/Df
A
B
C
DAPI Phalloidin D1
Spermatogonia
Control
D1EY05004/Df
Spermatocytes
Control
D1LL03310/Df
Accessory Gland
Control
D1LL03310/Df
D
E
F
G
H
I
DAPI Vasa AATAT
DAPI Vasa AATAT
DAPI AATAT
siControl
siHMGA1
J
K
DAPI Major Satellite
L
p=0.0023
% chr. disruption
50
40
30
20
10
0
siCtrl
siHMGA1

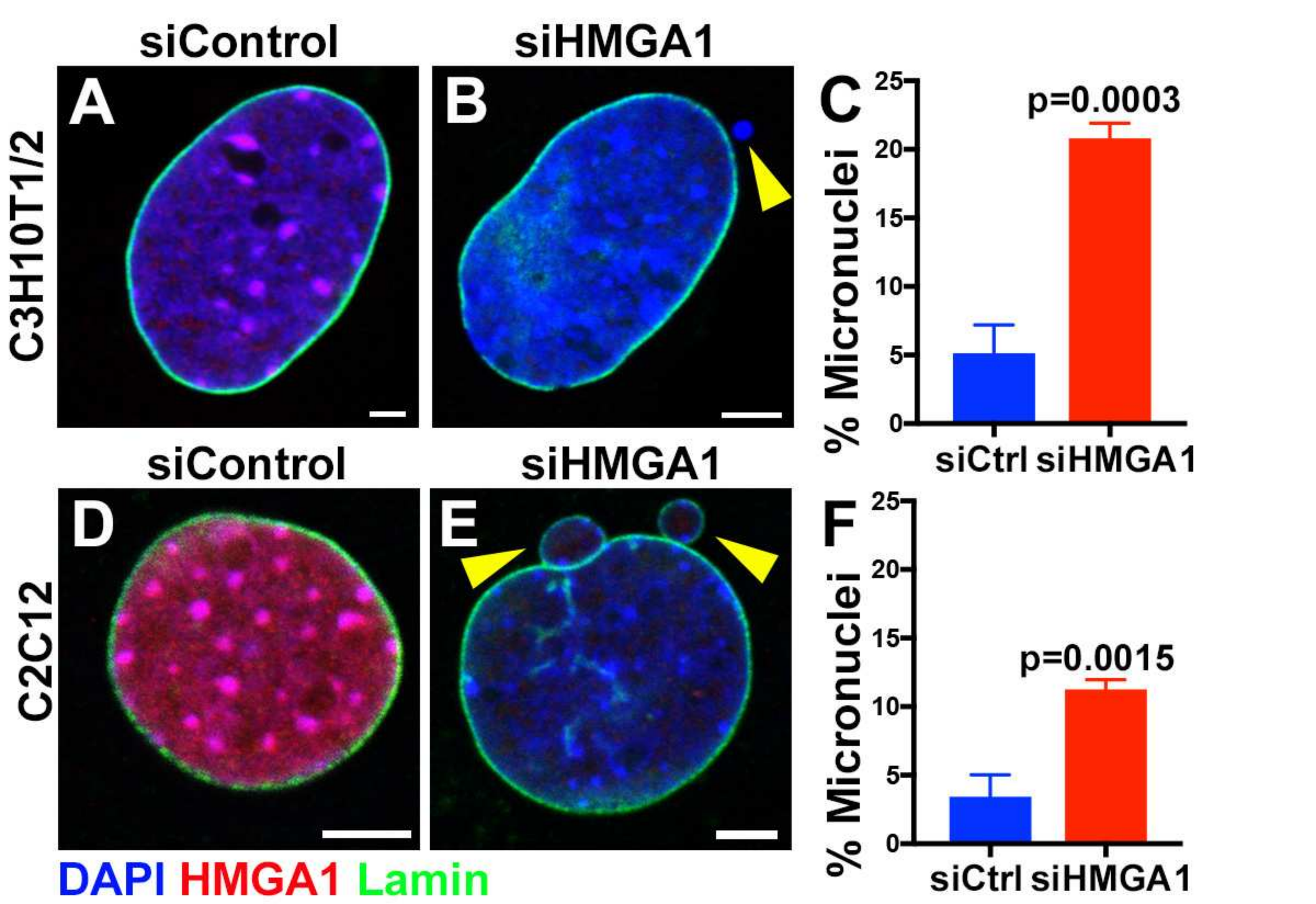
siControl
siHMGA1
C3H10T1/2
A
B
C
% Micronuclei
p=0.0003
siCtrl
siHMGA1
siControl
siHMGA1
C2C12
D
E
F
% Micronuclei
p=0.0015
siCtrl
siHMGA1
DAPI HMGA1 Lamin

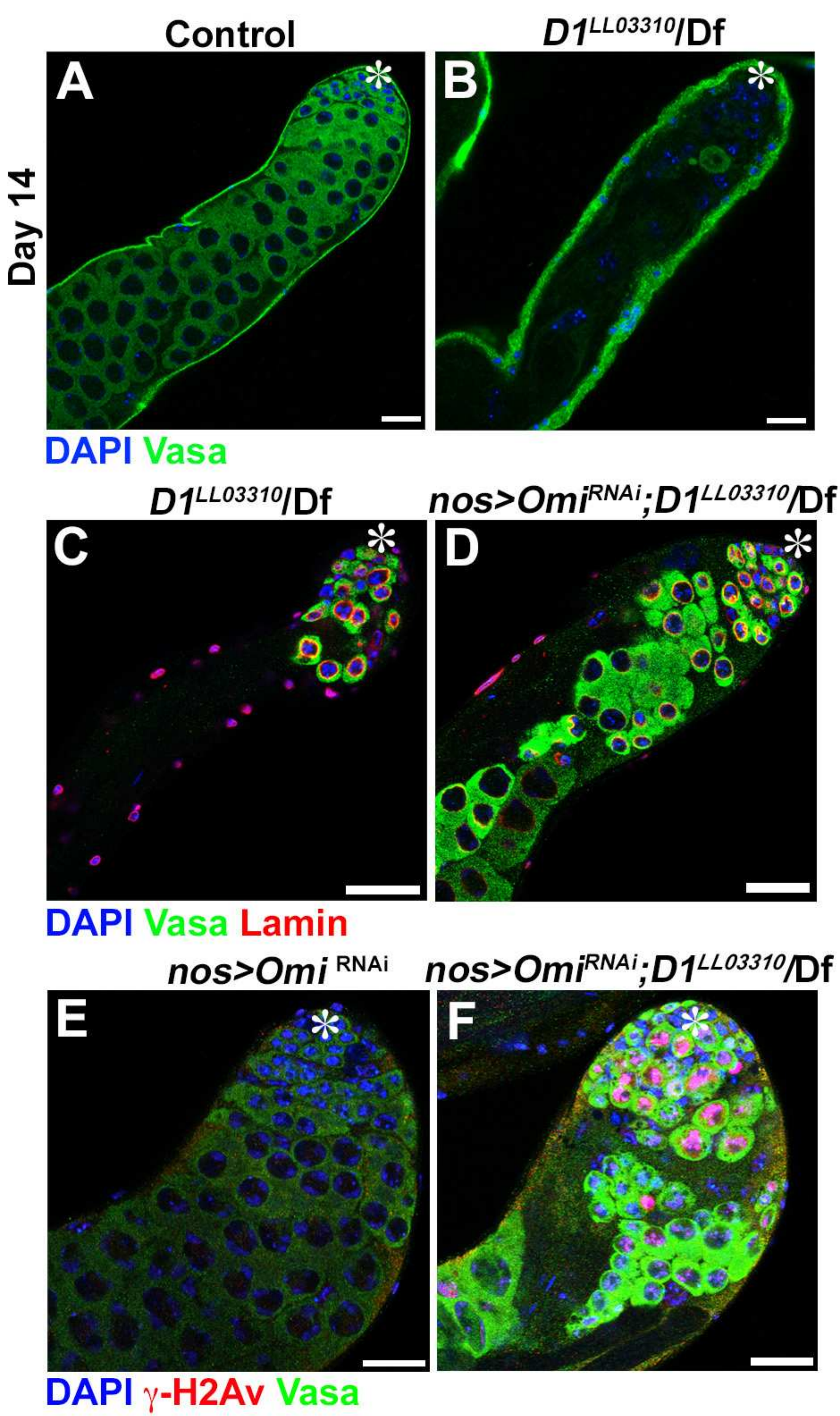
Control
D1LL03310/Df
Day 14
A
B
DAPI Vasa
D1LL03310/Df
nos>OmiRNAi;D1LL03310/Df
C
D
DAPI Vasa Lamin
nos>Omi RNAi
nos>OmiRNAi;D1LL03310/Df
E
F
DAPI γ-H2Av Vasa

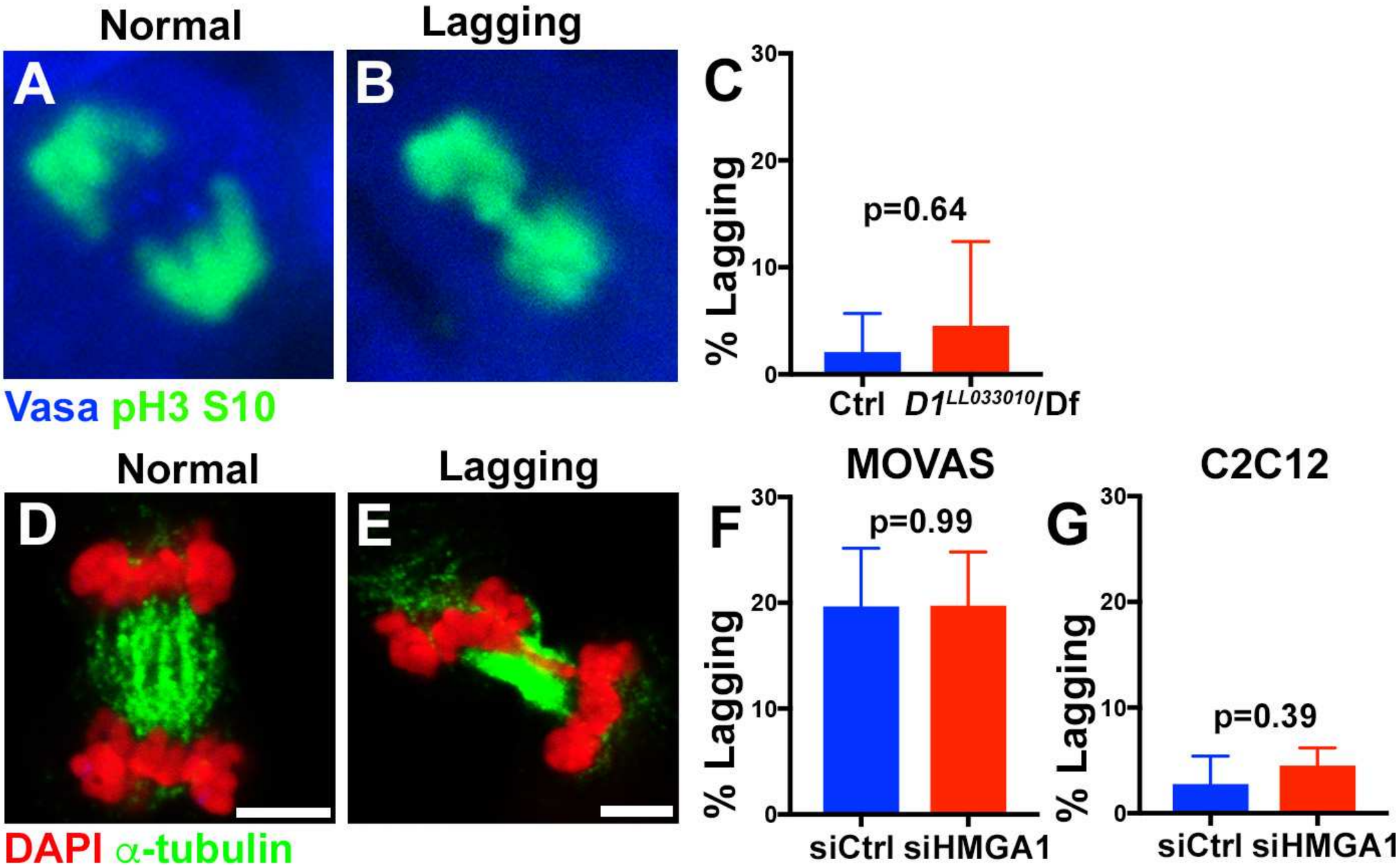
Normal
Lagging
A
B
Vasa pH3 S10
C
% Lagging
30
20
10
0
p=0.64
Ctrl
D1LL033010/Df
Normal
Lagging
D
E
DAPI α-tubulin
MOVAS
F
% Lagging
30
20
10
0
p=0.99
siCtrl
siHMGA1
C2C12
G
% Lagging
30
20
10
0
p=0.39
siCtrl
siHMGA1